Charles University in Prague
Faculty of Mathematics and Physics

BACHELOR THESIS

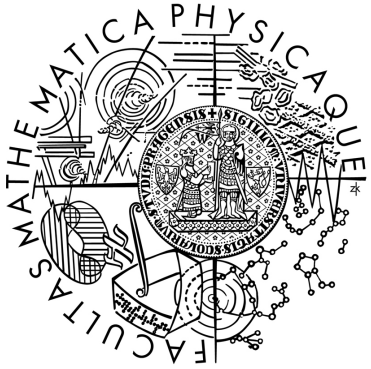

Tamara Skokánková

Low Frequency Oscillatory Flow of Cryogenic Helium

Department of Low Temperature Physics

Supervisor of the bachelor thesis: RNDr. David Schmoranzer, Ph.D.

Study programme: Physics
Specialization: General Physics

Prague 2014

First and foremost, I would like to thank my parents, who have taught me to believe and to question. Further, I owe many thanks to all my friends, who have shown their support during the completion of this thesis and in other times of need. Finally, I would like to express my sincere gratitude to my supervisor, RNDr. David Schmoranzer, PhD. for his invaluable help during the experiments, data processing and interpretation as well as for his corrections, patience, motivation and enthusiasm. The other main person, who affected this thesis, has been my senior colleague and consultant Dr. Martin Jackson, Ph.D. who lent me a lot of books and helped me with the measurements and the language aspect of my thesis.

I declare that I carried out this bachelor thesis independently, and only with the cited sources, literature and other professional sources.

I understand that my work relates to the rights and obligations under the Act No. 121/2000 Coll., the Copyright Act, as amended, in particular the fact that the Charles University in Prague has the right to conclude a license agreement on the use of this work as a school work pursuant to Section 60 paragraph 1 of the Copyright Act.

In Prague date..... signature

Název práce: Nízkofrekvenční oscilační proudění kryogenního hélia

Autor: Tamara Skokánková

Katedra / Ústav: Katedra fyziky nízkých teplot

Vedoucí bakalářské práce: RNDr. David Schmoranzer, Ph.D.

Abstrakt:

Tato práce je založena na zopakování experimentu, který provedli R. J. Donnelly and A. C. Hollis Hallett v roce 1958. Bylo provedeno měření pohybu torzně oscilujícího disku v supratekutém heliu při teplotách v rozmezí 1.37 až 2.16 K za tlaku nasycených par. Byly naměřeny časové průběhy úhlové rychlosti disku a určeny kritické hodnoty amplitudy úhlové rychlosti. Získané teplotní závislosti ukázaly, že naměřené nelineární síly pocházejí nejspíše od supratekuté složky. Na základě těchto měření byl navržen scénář přechodu k turbulenci v proudění vyvolaném torzně oscilujícím diskem.

Klíčová slova:

supratekuté helium, dvousložkový model, torzní oscilace, kvantované víry

Title: Low Frequency Oscillatory Flow of Cryogenic Helium

Author: Tamara Skokánková

Department / Institute: Department of Low Temperature Physics

Supervisor of the bachelor thesis: RNDr. David Schmoranzer, Ph.D.

Abstract:

This work is based on the experiment that was carried out by R. J. Donnelly and A. C. Hollis Hallett in 1958. Measurements were carried out with a torsionally oscillating disc in superfluid helium over a temperature range of 1.37 to 2.16 K at saturated vapor pressure. We were able to measure time dependences of the angular velocity of the disc and to determine critical values of the angular velocity amplitude. The obtained temperature dependences also show that the measured nonlinear forces originate from the superfluid component. Based on these measurements, a model describing the mechanisms of the transition to turbulence in a flow due to a torsionally oscillating disc is proposed.

Keywords:

superfluid helium, two-fluid model, torsional oscillation, quantized vortices

Contents

Introduction

The beginning of low-temperature physics can be traced back to July 10 1908, when the Dutch physicist Heike Kamerlingh Onnes liquefied helium for the first time in Leiden. After a series of experiments that followed over the years, low-temperature physicists knew that helium had remarkable properties which could not be explained by classical physics. It was clear that the behaviour of helium at temperatures above and below 2.17 K clearly differed. This temperature was named the λ-point because of the shape of the temperature dependence of the specific heat. Helium above and below this temperature was named He I and He II, respectively.

In 1938, Pyotr Kapitsa published the results of his hydrodynamic experiments with liquid helium [1]. Kapitsa observed that, although the flow of Helium in a gap between two optical-grinded discs is barely detectable after cooling below the λ-point, it may flow smoothly. This phenomenon was dubbed superfluidity.

Kapitsa's and later, Allen's and Misener's experiments [2] showed the dynamic viscosity of superfluid helium was significantly lower than the dynamic viscosity of normal liquid helium. However, experiments on torsionally oscillating cylinders in Toronto [3] showed that He II is able to flow without internal friction in certain cases, but in others, it appeared to behave as a normal viscous liquid. This was a serious problem which had to be resolved.

A milestone in resolving these conflicting experiments was achieved by Andronikashvili [4]. He used an assembly of discs stacked very close to each other immersed in liquid helium and measured the resonant frequency of torsional vibrations in relation to temperature. The resonant frequency was found to be almost constant in He I, while in He II, it increased noticeably. This experimental result lead to Landau's phenomenological two-fluid description of He II [5; 6], which tells us that He II behaves as a mixture of two independent components – a normal and a superfluid component.

The last experiment relevant to my thesis was performed R. J. Donnelly and A. C. Hollis Hallett in 1958 [7]. In this experiment, a torsion oscillator consisting of a suspended disc was used to explore the flow of superfluid helium. My work is based on repeating their experiment using modern technology, such as imaging and data processing, which could provide more accurate results.

The Joint Low Temperature Laboratory established between the Faculty of Mathematics and Physics of Charles University in Prague and the Institute of Physics of the Academy of Sciences of the Czech Republic, where this work has been performed, has extensive experience in the exploration of He II using various oscillating bodies, like quartz tuning forks [8; 9; 10]. For this reason, I will compare the results of my work using a torsion oscillator with the results of my colleagues using other oscillators in He II.

1 Theoretical Background

To plan our experiment, as well as the processing and interpretation of any measured quantities, it is necessary to have certain knowledge of the following fields of physics: classical hydrodynamics, superfluidity and the behaviour of torsional oscillators in fluids.

1.1 Selected Parts of Classical Hydrodynamics

To study the motion of the continuum, we can basically use two methods. The continuum can be divided into individual material points (volume elements), and track their movement – this is known as Lagrange's method. We can also focus on the points of space and monitor the movement of the alternating material points of the continuum in which these points of space enter – this is the Euler's method.

Following Euler, we can describe the motion of fluids by deriving the equations of motion. The entire derivation can be found in ref. [11] on pages 44 – 46. The equation of motion of an incompressible viscous fluid can be written in the form:

$$\frac{\partial \vec{u}}{\partial t} + \vec{u} \cdot \nabla \vec{u} = -\frac{1}{\rho} \nabla p + \nu \Delta \vec{u} + \vec{f}, \tag{1}$$

where $\vec{u}$ is velocity, t time, ρ density of the fluid, p is pressure, ν kinematic viscosity, and $\vec{f}$ is the sum of the forces acting on the fluid. This equation is called the Navier-Stokes equation. [11]

To fully describe the motion of fluids, it is required to supplement this equation with the continuity equation:

$$\frac{\partial \rho}{\partial t} + \nabla \cdot \vec{j} = 0, \tag{2}$$

where $\vec{j} = \rho \vec{u}$ is flux density of the fluid. This equation can be easily inferred from Gauss's theorem. The derivation can be found in ref. [11] on pages 1 and 2.

Although this equation system describes the mechanical behaviour of incompressible viscous fluids, an analytical solution exists only for some simple cases of flows. In more complex cases, it is necessary to solve the system numerically. Whether or not there are any analytical solutions depends on the following flow characteristics.

Time dependent flow variables can be divided into two categories; stable (stationary) and unsteady (transient) flows. Stationary flow variables at a given point of the liquid are time-independent, whereas in the case of unsteady (transient) flows, the flow variables are time-dependent.

Accordingly, the motion of viscous fluid flow can be divided into two basic types: laminar and turbulent flow. In the case of laminar flow, the fluid particles move next to each other as if in layers that cannot mix. In turbulent flow, fluid particles carry the flow in addition to shifting and complex motion, which leads to the formation of vortices and the liquids mixing. The velocity of the individual fluid particles varies irregularly. Particles no longer have a constant velocity at all locations, so the turbulent flow is not stationary.

Whether a (statistically) steady flow is laminar or turbulent depends on the Reynolds number *Re*:

$$Re = \frac{Ul}{\nu}, \tag{3}$$

where U is the mean velocity of the flow, l is the scale at which velocity changes occur (typically the size of a submerged body or the radius of a pipe) and ν is the kinematic viscosity. If the Reynolds number is smaller than a critical value, which must be determined for each type of flow experiments, the flow is laminar. If the Reynolds number is greater than this critical value, the flow is turbulent.

Characteristic numbers such as *Re* express the dynamical similarity of different flows. Two flows are dynamically similar only if they are similar geometrically and the appropriate characteristic numbers have the same value.

To characterise a steady flow, just one characteristic number is required. To characterise unsteady flows, it is necessary to add another characteristic number to the parameters describing stationary flow that would reflect the time-dependence or periodicity of the flow. Thus, periodic flows are dynamically similar if two corresponding characteristic numbers are equal.

To the Reynolds number one might, for example, add the Strouhal number *Sr*:

$$Sr = \frac{f_V D}{U}, \tag{4}$$

which relates the frequency of the formation of vortices in the wake behind an obstacle f_V, its characteristic size D, and velocity, U. Other frequently used characteristic numbers are the Stokes and the Keulegan-Carpenter numbers.

The Stokes number β, corresponds to the ratio of the characteristic body dimension D, to the viscous penetration depth δ and is defined by the following formula

$$\beta = \frac{fD^2}{\nu} = \frac{1}{\pi}\frac{D^2}{\delta^2}, \tag{5}$$

where ν is the kinematic viscosity of the fluid and f is the frequency of oscillation. The Keulegan-Carpenter number K_C, describes the relative importance of the non-linear drag forces over inertial forces for bluff objects in an oscillatory fluid flow or similarly, for objects that oscillate in a fluid at rest. It is defined by the formula:

$$K_C = \frac{UT}{l} = \frac{2\pi U}{\omega l}, \tag{6}$$

where U is the velocity amplitude, T is the period of the oscillation and l is a characteristic length scale.

These pairs of numbers are just the most frequently used combinations, but in principle, we can choose different pairs because it is possible to roam freely between the characteristic numbers.

Note that if we substitute $l = D$, assuming that the velocity changes typically at the length scales corresponding to the body size, the following relation holds between the dimensionless numbers: $\beta K_C = Re$. This is valid at low frequencies (low Stokes number), where the viscous penetration depth is much larger than the body dimensions.

It is of interest that in the high frequency limit ($\beta \gg 1$), only one characteristic number is required to describe the flow. Let us examine why it is possible to say that. Consider the Navier-Stokes equation, neglecting the volume forces $\vec{f}$, and put it into a dimensionless form using the following relations:

$$\vec{u} = U\overrightarrow{u'}, \qquad \vec{\nabla} = \frac{1}{l}\overrightarrow{\nabla'}, \qquad t = \frac{1}{\omega}t', p = \rho U^2 p', \tag{7}$$

where U is the velocity amplitude, l some characteristic length at which the velocity is changing, ω is the angular frequency and the dashed quantities are the dimensionless counterparts. After multiplying by l/U^2, we obtain the dimensionless form of the Navier-Stokes equation:

$$\frac{l\omega}{U}\frac{\partial\overrightarrow{u'}}{\partial t'} + \overrightarrow{u'}\cdot\nabla'\overrightarrow{u'} + \nabla' p' = \frac{\nu}{Ul}\Delta'\overrightarrow{u'}. \tag{8}$$

There are two prefactors in the dimensionless equation: $(l\omega)/U$ and $\nu/(Ul)$, which completely characterise the flow. The first one is the inverse

Keulegan-Carpenter number multiplied by 2π and the second is the inverse Reynolds number.

However, in the limit of high frequencies, more significant velocity changes occur on the length scale of the viscous penetration depth $\delta = \sqrt{2\nu/\omega}$ than on the scale of the body dimensions, as for sufficiently high frequencies, we have $\delta \ll l$ [11]. Therefore, we will substitute δ for the characteristic length scale l, and we will show that the two characteristic prefactors are equal, except for a multiplier constant. After substituting the formula for the viscous penetration depth, the first prefactor is given by:

$$\frac{2\pi}{Kc} = \frac{l\omega}{U} = \frac{\omega\sqrt{\frac{2\nu}{\omega}}}{U} = \sqrt{2}\frac{\sqrt{\nu\omega}}{U} \tag{9}$$

whilst the second is given by:

$$\frac{1}{Re} = \frac{\nu}{Ul} = \frac{\omega}{U\sqrt{\frac{2\nu}{\omega}}} = \frac{1}{\sqrt{2}}\frac{\sqrt{\nu\omega}}{U}. \tag{10}$$

Equivalently, it is possible to say that $K_C = \pi Re$ in the limit of high frequencies, which replaces the relation $K_C\beta = Re$, valid in the low frequency limit.

The fact that both terms characterizing the flow in the dimensionless Navier-Stokes equations are directly proportional in the limit of high frequencies, allows us to describe a flow only by one characteristic number. For this purpose, we shall choose the Reynolds number using δ for the characteristic length scale, similarly to the above calculation. We therefore define $Re_\delta = U\delta/\nu = U\sqrt{2/\nu\omega}$, understanding that (given the geometry of the oscillator and the bounding volume including their surface roughness); this is the only dimensionless parameter determining the oscillatory flow in the high frequency limit.

1.2 Liquid Helium and the Basics of Superfluidity

Helium is the second most abundant element in the universe. Its atomic number is 2; it is an inert, tasteless, odourless gas. It has two stable isotopes; ^{4}He and ^{3}He. Helium has the lowest temperature of liquefaction at atmospheric pressure and displays unique behaviour in the liquid state. Helium is the only known liquid that undergoes a superfluid phase transition. Normal liquid helium and cooled helium gas are classical Newtonian fluids with the lowest kinematic viscosity of all known substances. For cold helium gas, it has a value of 3.21×10^{-8} $m^{2}\cdot s^{-1}$ at a pressure of 2.5 bar and a temperature of 5.5 K. For normal liquid helium, it is 1.96×10^{-8} m^2s^{-1} at saturated vapour pressure and at a temperature of 2.25 K. For comparison, the kinematic viscosity of water at 298.15 K is 1.016×10^{-6} m^2s^{-1}.

Let us examine the differences between the stable helium isotopes. ^{3}He is a rare isotope, in nature there are one million atoms of ^{4}He to every atom of ^{3}He. Although the two isotopes of helium behave similarly under normal conditions, they behave very differently under extreme conditions, such as low temperatures. This is due to the spin of the atoms governed by the number of nucleons in them. ^{4}He atoms have four nucleons, therefore they are indistinguishable particles with integer spin - bosons and their behaviour is governed by Bose-Einstein statistics. In contrast, the ^{3}He atom has three nucleons and is a representative of indistinguishable particles with half-integer spin - Fermions and obeys Fermi-Dirac statistics. The difference of these statistics is highlighted under extreme conditions and results in the helium isotopes having different behaviour with varying temperature as well as the nature of the transition into the superfluid phase. The temperature of the superfluid transition in ^{4}He is around 2.17 K at saturated vapour pressure. In the case of ^{3}He, this phase transition occurs at temperatures between 0.93 mK and 2.7 mK, in the pressure range 0 to 34.5 bar. Throughout this discussion, we will only consider ^{4}He and its superfluidity.

The uniqueness of ^{4}He is evident from its phase diagram (Fig. 1.1). Unlike other substances, ^{4}He has no triple point, or indeed any sublimation curve. During cooling at atmospheric pressure, helium will not freeze, even if the sample were cooled down to absolute zero. To form solid ^{4}He, an external pressure of at least 25 atmospheres is required.

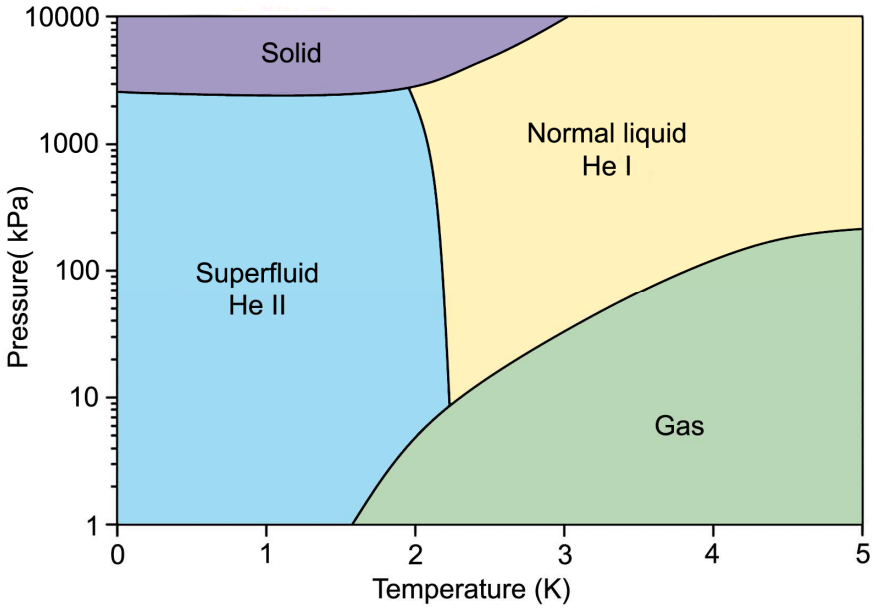

Fig. 1.1: The phase diagram of ^{4}He.

Helium-4 in the superfluid phase (He II) gives us a wonderful opportunity to observe the direct manifestations of quantum physics on a macroscopic scale. It was the first substance found to undergo a superfluid transition, and as such, it was the first superfluid to be studied in detail.

In the phase diagram, normal He I and superfluid helium He II are separated by the so-called λ-line, where the transition between the two fluids occurs. While looking into a glass cryostat containing liquid helium, the temperature is reduced along the saturated vapour curve by gradually pumping on the bath, the transition to the superfluid state is clearly evident. Suddenly, the heavy boiling of the liquid is completely suppressed. This phenomenon occurs due to the high thermal conductivity of He II, which is at least 3 million times higher than in He I and is sufficiently high to suppress the thermal gradients necessary for the existence of nucleation sites where bubbles form. Thus, a volume of He II is not cooled by boiling, but rather by superficial evaporation only. Furthermore, if we prevent the influence of mechanical vibrations, the surface of the He II is smooth to the level of one atomic layer, which is the smoothest naturally occurring surface.

Another feature of He II is the ability to adhere to almost any contact material to create a nanoscopic layer on its surface – the superfluid film [12]. This feature is manifested in the phenomena known as thin film flow. If a tube is partially

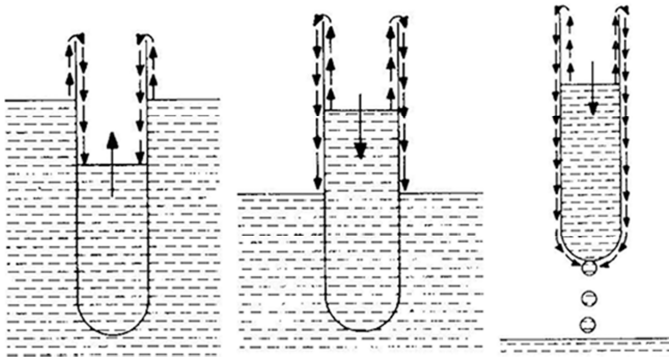

Fig. 1.2: Manifestation of the superfluid film.

submerged in a bath of superfluid helium, in time, it will itself be filled up to a height which corresponds to the level of the surrounding liquid bath (Fig. 1.2). If this tube is raised slightly above the surface of the bath, the liquid in the tube will then start to flow back into the bath through the superfluid film. If the tube were to be removed from the superfluid helium bath entirely, one could observe the formation of helium droplets on the bottom of the tube which drip back into the bath and the tube empties itself over time.

In experiments where thermal gradients are induced, more unusual properties of He II can be observed, e. g. the fountain effect [13]. Due to this effect, it is possible to observe how the superfluid component of He II leaks through a labyrinth of very narrow channels through which the normal fluid, which has a finite viscosity, flows only with great difficulty, if at all. Such devices can be made of sintered metals and are known as superleaks. It was demonstrated that a temperature increase would also result in an overpressure that will propel the contained fluid upward in a fountain jet (Fig. 1.3). There is also the opposite so-called mechano-caloric effect. Thus, in superfluid helium, any temperature gradient corresponds to a pressure gradient and vice versa.

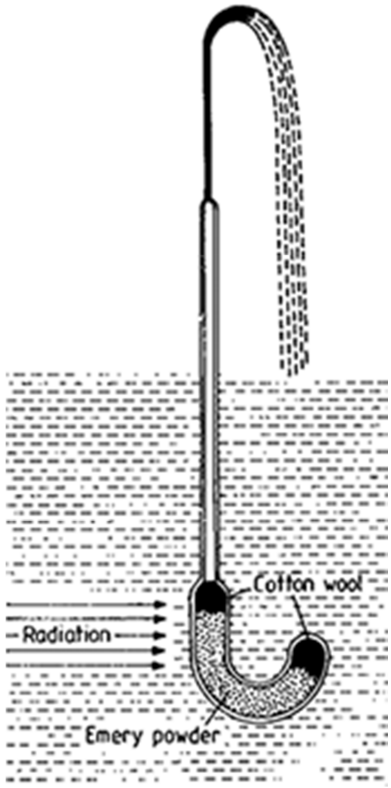

Fig. 1.3: The fountain effect.

As mentioned above, during the 1930s, the results related to the viscosity of He II were controversial. The results obtained by Allan and Misener [2] on capillary flow and from Kapitza's experiments [1] with a chamber closed by optically smooth discs (Fig. 1.4), indicated that the viscosity of He II

is approximately 1500-times lower than that of the He I. In contrast, earlier work based on torsional oscillations of a cylinder suggested a viscosity comparable with He I.

These seemingly contradictory results together with the other anomalous properties, outlined above, stimulated the first attempts of Tisza and Landau towards a theoretical description of He II. However, it was not until the work of Andronikashvili that the situation became somewhat clearer.

Andronikashvili [4] used a system of discs suspended by a fibre under tension made from phosphor bronze which had a diameter of 340 μm and a length of approximately 100 cm (Fig. 1.4). The stack consisted of 100 discs of 0.013 mm thick aluminium foil, interleaved 0.21 mm thick aluminium washers strung onto an aluminium mandrel. When we submerge the stack of discs into liquid helium, the viscous penetration depth will be greater than the spacing of discs and the liquid will be clamped by the oscillator. The moment of inertia in a viscous fluid will be affected by the moment of inertia in vacuum and the oscillation period will be greater because of the increase of effective mass. Andronikashvili observed that upon cooling below the superfluid transition temperature, the period of oscillation significantly decreased.

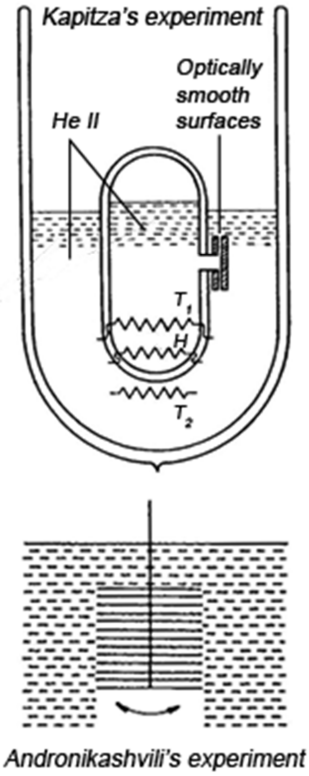

Fig. 1.4: Diagram of Kapitza's (top) and Andronikashvilli's (bottom) experiments.

The observation that a portion of the fluid between the discs mechanically "decoupled" from the oscillator, led to the idea that He II consists of two components, one of which flows without friction, and that their ratio depends strongly on the temperature. This of course explains the previous controversy, since both components contribute to the friction acting on a torsionally oscillating cylinder, but only the superfluid component with zero viscosity can flow through tiny capillaries, or into Kapitza‘s experimental chamber. Eventually, the phenomenological two-fluid model was formulated, as we still use it today.

This model describes He II as a fluid composed of two components called the normal and superfluid components. The normal component has a finite viscosity,

transfers heat and has finite entropy. The superfluid component has zero viscosity, cannot transmit heat and has no entropy. These two components occupy the same space and are considered to have independent velocity fields. The density of He II, ρ is given by the sum of the densities of the two components, i.e., $\rho = \rho_n + \rho_s$, where ρ_n is the density of normal component and ρ_s is the density of superfluid component (Fig. 1.5).

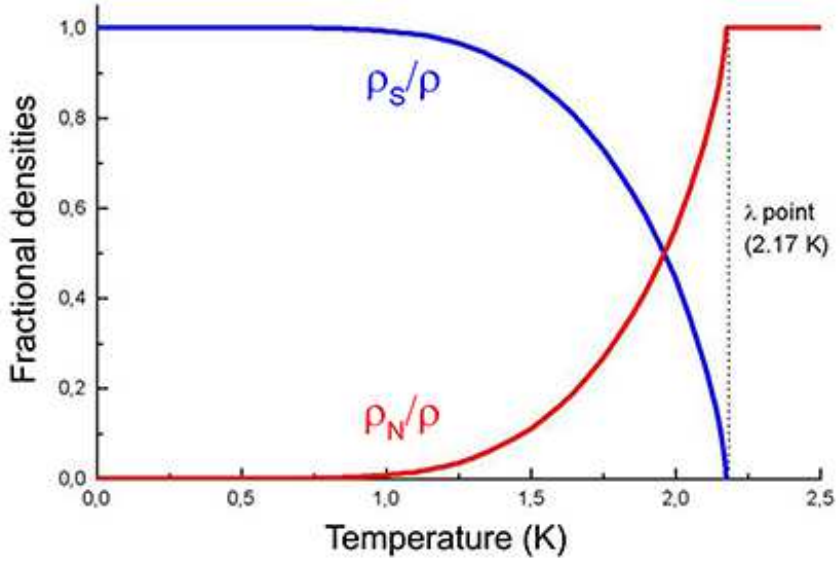

Fig. 1.5: The dependence of the densities of the normal and superfluid components on temperature.

The ratio of the normal and superfluid component is only dependent on temperature (and pressure). When we move along the saturated vapour curve from the lambda point to lower temperatures, the ratio of the densities shifts rapidly in favour of the superfluid component. Because the normal component density decreases, the viscous forces acting on the surface of a body immersed will come from a lesser part of He II.

The derivation of the hydrodynamic equations of the two-fluid model is quite complex. It can be found, for example, in ref. [14]. The linearised form of the dynamic equations for an incompressible flow at low counterflow velocities is as follows:

$$\rho_s \frac{\partial \overrightarrow{u_s}}{\partial t} + \rho_s (\overrightarrow{u_s}\nabla)\overrightarrow{u_s} = -\frac{\rho_s}{\rho}\nabla p + \rho_s S \nabla T - \overrightarrow{F_{ns}}, \tag{11}$$

$$\rho_n \frac{\partial \overrightarrow{u_n}}{\partial t} + \rho_n (\overrightarrow{u_n}\nabla)\overrightarrow{u_n} = -\frac{\rho_n}{\rho}\nabla p - \rho_s S \nabla T + \overrightarrow{F_{ns}} + \eta \nabla^2 \overrightarrow{u_n}, \tag{12}$$

where η is the dynamic viscosity of the normal component and $\overrightarrow{F_{ns}}$ is a term representing the coupling force of mutual friction between the normal and superfluid components, if vortices are present in the superfluid. These need to be supplemented by an equation of continuity, for incompressible flow, this is given by:

$$\nabla \cdot (\rho_n \overrightarrow{u_n} + \rho_s \overrightarrow{u_s}) = 0, \tag{13}$$

and if we choose to neglect any energy dissipation, we also need an equation expressing the law of the conservation of entropy given by:

$$\frac{\partial(\rho s)}{\partial t} + \nabla \cdot (\rho s \overrightarrow{u_n}) = 0, \tag{14}$$

where *s* is the specific entropy and $\rho s \overrightarrow{u_n}$ expresses the entropy flux.

If we assume that there are not any vortices in the liquid, we can neglect the mutual friction term and if we consider the flow to be isothermal, the equations will be reduced to their simplest form:

$$\rho_s \frac{\partial \overrightarrow{u_s}}{\partial t} + \rho_s (\overrightarrow{u_s} \nabla) \overrightarrow{u_s} = -\frac{\rho_s}{\rho} \nabla p, \tag{15}$$

$$\rho_n \frac{\partial \overrightarrow{u_n}}{\partial t} + \rho_n (\overrightarrow{u_n} \nabla \overrightarrow{u_n}) = -\frac{\rho_n}{\rho} \nabla p + \eta \nabla^2 \overrightarrow{u_n}, \tag{16}$$

The first of these is the Euler equation for the superfluid component, and the second is the Navier-Stokes equations for the viscous normal component. These equations are no longer coupled, so the velocity fields of the two components are in the simplest case, independent.

In his two-fluid model, Landau assumed that the normal component consists of thermally exited helium atoms, and proposes a description using the dispersion relations of thermal excitations. His dispersion relation showed two types of excitations called "phonons" and "rotons." Parameters depending on the momentum and energy were chosen to match the data measured by Andronikashvili because the number density of phonons and rotons can be used to estimate the density of the normal component.

Another important result that can be derived from the correct form of the excitation spectra predicted by Landau is the ultimate critical velocity above which superfluidity in He II is no longer possible. Considering the change of dispersion relations in the Galilean transformation in the reference system of a moving body, we come to the same conclusion as Landau did that excitations

(rotons) will form continuously at velocities above 59 meters per second. This velocity value was later confirmed by ions moving in He II. [15]

As it has two independent components, He II supports some regimes of flow which cannot exist in conventional liquids. For example, turning on a heater at a closed end of a channel causes the superfluid component to flow toward the heater where it absorbs heat and changes into the normal component, which must then flow in the opposite direction, away from the heater. A class of similar phenomena is known as thermal counterflow. This is characterised by zero mass transfer, but at sufficiently high velocities it leads to the formation of turbulence.

The two-fluid model works well in the temperature range from the lambda point down to 1 K, where the normal component is already quite depleted. At temperatures below 0.7 K, the model fails completely, because there is so little normal component that it no longer represents a continuum, but must be described as ballistic thermal excitations. At temperatures below 0.2 K, the hydrodynamics of He II does not significantly change any more and we talk about the limit of zero temperature.

While Landau [5; 6] published his phenomenological two-fluid model, Fritz London [16] and Laszlo Tisza [17] worked on the theory based on the Bose-Einstein condensation (BEC), which would explain the non-classical properties of He II. BEC is a process in which bosons will occupy the fundamental quantum-mechanical state (the lowest accessible energy state) on a macroscopic scale if they are cooled to a sufficiently low temperature, provided there is a sufficient density. Fritz London calculated that for an ideal gas composed of (non-interacting) helium atoms, the condensation should occur at 3.15 K, which is sufficiently close to the experimentally determined temperature, 2.17 K corresponding to the superfluid phase transition. The difference arises from the fact that atoms in liquid helium in fact interact rather strongly, whereas Fritz London’s calculation assumes no interactions at all.

With this approach, it was possible to explain the fountain and mechano-caloric effects, since any temperature gradient in the newly formed condensate automatically implies a pressure gradient, and vice versa. Furthermore, it was assumed that the superfluid component consists of the atoms forming the Bose-Einstein condensate, while the rest of the atoms constitute the "normal component." However,

Landau's model was more successful in describing the densities of the two components as inferred from Andronikashvili's experiment.

On the other hand, without a theory based on Bose-Einstein condensation, another peculiarity of He II - the existence of quantized vortices in the superfluid component – could not be explained. BEC theory suggests that the atoms in the ground state should be described by a single macroscopic quantum-mechanical wave function. If we try to calculate the velocity of the superfluid component, we find that no rotational movement should be possible, as the circulation around a loop bounding a continuous area of superfluid would be, by definition, zero. This is in contradiction with the experiment described in ref. [18], as uniform rotation of He II has been observed to be very similar to that in classical fluids.

This discrepancy can be resolved if we consider that rotation in He II creates one-dimensional topological defects (lines), along which a violation of superfluidity occurs. These defects have been observed experimentally and are called quantized vortices, as follows from the theory that the circulation of the superfluid component around these lines can only have defined (quantized) values, which are equal to multiples of the quantum of circulation $\kappa = h/m$, where h is Planck's constant and m the atomic mass of ^{4}He.

All quantized vortices in He II almost always have only one quantum of circulation, as this minimises the energy of the system. A complex tangle of these quantized vortices, which may arise at sufficiently high velocity, is called quantum turbulence.

1.3 Behaviour of a Torsionally Oscillating Disc in a Fluid

To compare our results with the theory of the hydrodynamics of superfluids, it is necessary to derive the theoretical description of the studied problem, the torsionally oscillating disc. Generally, finding solutions to the Navier-Stokes equations describing the behaviour of a fluid around an oscillating disc is a complex mathematical task. For turbulent flow, no solution can be derived analytically; even numerical simulations of such time-dependent flow would be of great complexity. Therefore, we limit ourselves to laminar flow and two simplified cases; flow around a torsional oscillator in the form of a disc placed in infinite volume of fluid and between two stationary parallel plates.

For this calculation, it is appropriate to start from the Navier-Stokes equations and the equation of continuity detailed in cylindrical polar coordinates r, φ, z. Then, the three components of the Navier-Stokes equation are as follows:

$$\frac{\partial u_r}{\partial t} + (\vec{u}\cdot\vec{\nabla})u_r - \frac{u_\varphi^2}{r} = -\frac{1}{\rho}\frac{\partial p}{\partial r} + \nu\left(\Delta u_r - \frac{2}{r^2}\frac{\partial u_\varphi}{\partial \varphi} - \frac{u_r}{r^2}\right), \tag{17}$$

$$\frac{\partial u_\varphi}{\partial t} + (\vec{u}\cdot\vec{\nabla})u_\varphi + \frac{u_r u_\varphi}{r} = -\frac{1}{\rho r}\frac{\partial p}{\partial \varphi} + \nu\left(\Delta u_\varphi + \frac{2}{r^2}\frac{\partial u_r}{\partial \varphi} - \frac{u_\varphi}{r^2}\right), \tag{18}$$

$$\frac{\partial u_z}{\partial t} + (\vec{u}\cdot\vec{\nabla})u_z = -\frac{1}{\rho}\frac{\partial p}{\partial z} + \nu\Delta u_z. \tag{19}$$

where

$$(\vec{u}\cdot\vec{\nabla})f = u_r\frac{\partial f}{\partial r} + \frac{u_\varphi}{r}\frac{\partial f}{\partial \varphi} + u_z\frac{\partial f}{\partial z}, \tag{20}$$

$$\Delta f = \frac{1}{r}\frac{\partial}{\partial r}\left(r\frac{\partial f}{\partial r}\right) + \frac{1}{r^2}\frac{\partial^2 f}{\partial \varphi^2} + \frac{\partial^2 f}{\partial z^2}, \tag{21}$$

and the equation of continuity is:

$$\frac{1}{r}\frac{\partial (r u_r)}{\partial r} + \frac{1}{r}\frac{\partial u_\varphi}{\partial \varphi} + \frac{\partial u_z}{\partial z} = 0. \tag{22}$$

Firstly, we will derive expressions describing the motion of a torsionally oscillating disc in infinite space.

Consider a plane disc with large radius R which executes rotary oscillations with a small amplitude about its axis, the angle of rotation being $\theta = \theta_0\cos(\omega t)$, where $\theta_0 \ll 1$. For small amplitude oscillations, the term $(\vec{u}\cdot\vec{\nabla})f$ in the equation of motion is always small compared with $\partial\vec{u}/\partial t$, whatever the frequency ω.

If $R \gg \delta$, i.e., if the radius significantly exceeds the viscous penetration depth, the disc may be regarded as infinite in determining the velocity distribution. It is easy to see that the solution of the Navier-Stokes equation is such that $u_r = u_z = 0$, $u_\varphi = u = r\Omega(z,t)$, where $\Omega(z,t)$ is the angular velocity of the fluid. Then the equation of continuity is satisfied identically and the three components of the Navier-Stokes equation in cylindrical polar coordinates are reduced to the single equation:

$$\frac{\partial \Omega}{\partial t} = \nu \frac{\partial^2 \Omega}{\partial z^2}. \tag{23}$$

The solution of this equation, which satisfies the boundary condition $\Omega = \Omega_D \equiv -\omega\theta_0 \sin(\omega t)$, where Ω_D is the angular velocity of the disc, for $z = 0$, and is equal to zero for $z = \infty$ is:

$$\Omega = -\Omega_0 e^{-\frac{z}{\delta}} \sin\left(\omega t - \frac{z}{\delta}\right), \tag{24}$$

where $\Omega_0 = \omega\theta_0$ is the amplitude of the angular velocity of the disc and δ is the viscous penetration depth.

The moment of the frictional forces on both sides of the disc is given by:

$$\begin{aligned} M &= 2\int_0^R \int_0^{2\pi} r F_v r d\varphi dr \\ &= 4\pi\eta \int_0^R r \left(\frac{\partial \vec{u}}{\partial z}\right)_{z=0} \mathrm{d}r \\ &= \frac{\pi}{\sqrt{2}} \Omega_0 \sqrt{\omega\rho\eta} R^4 \left(\cos(\omega t) + \sin(\omega t)\right), \end{aligned} \tag{25}$$

where F_v is the local viscous drag force given by $F_v = \eta \left(\frac{\partial \vec{u}}{\partial z}\right)_{z=0}$. However, only the part of the viscous force in-phase with the velocity is responsible for the damping of the oscillations. One can therefore write for the dissipative part of the moment of forces:

$$M_{dis} = \frac{\pi}{\sqrt{2}} \Omega_0 \sqrt{\omega\rho\eta} R^4 \sin(\omega t), \tag{26}$$

from which it is possible to calculate the damping coefficient k and its effective value k_{eff} given by averaging the dissipative forces over one period:

$$k = -\frac{M_{dis}}{\Omega} = \frac{\pi}{\sqrt{2}} \sqrt{\omega\rho\eta} R^4, \tag{27}$$

$$k_{eff} = \frac{k}{T}\int_0^T |\sin(\omega t)| = \frac{2}{\pi}k = \sqrt{2\omega\rho\eta}R^4, \tag{28}$$

which will be directly compared with experimental data.

A factor often used to describe the fluid flow is the rate of energy dissipation. It can be derived analogically to the dissipative moment of the frictional forces:

$$\varepsilon = -\frac{dE}{dt} = 2\int_0^R \int_0^{2\pi} u\, F_{v,dis}\, r d\varphi dr = \frac{\pi}{\sqrt{2}}{\Omega_0}^2\sqrt{\omega\rho\eta}R^4 \sin^2(\omega t), \tag{29}$$

where $F_{v,dis}$ is the dissipative component of the viscous force (in-phase with velocity). An effective energy dissipation averaged over one period is then given by:

$$\varepsilon_{eff} = \frac{\pi}{2\sqrt{2}}{\Omega_0}^2\sqrt{\omega\rho\eta}R^4. \tag{30}$$

The same procedure as above is used to derive the relations describing the flow around the torsionally oscillating disc placed in the middle of two plates located at distance h on either side of the disc. The calculation will differ mostly by the boundary conditions – In this case, it is required that the solution of this equation is $\Omega = -\Omega_0 \sin(\omega t)$ for $z = 0$ and $\Omega = 0$ for $z = h$. Relations describing the desired variables will take a slightly different shape then:

$$\begin{aligned}\Omega^\dagger = {} & \frac{\Omega_0}{\cosh\left(\frac{2h}{\delta}\right) - \cos\left(\frac{2h}{\delta}\right)} \\ & \cdot \left(\cos(\omega t)\left(\sinh\left(\frac{z}{\delta}\right)\sin\left(\frac{z-2h}{\delta}\right)\right.\right. \\ & \left. - \sin\left(\frac{z}{\delta}\right)\sinh\left(\frac{z-2h}{\delta}\right)\right) \\ & + \sin(\omega t)\left(\cosh\left(\frac{z}{\delta}\right)\cos\left(\frac{z-2h}{\delta}\right)\right. \\ & \left.\left. - \cos\left(\frac{z}{\delta}\right)\cosh\left(\frac{z-2h}{\delta}\right)\right)\right),\end{aligned} \tag{31}$$

$$\begin{aligned}M^\dagger = {} & \frac{1}{\sqrt{2}}\frac{\pi\Omega_0\sqrt{\omega\rho\eta}R^4}{\cosh\left(\frac{2h}{\delta}\right) - \cos\left(\frac{2h}{\delta}\right)} \\ & \cdot \left(\sinh\left(\frac{2h}{\delta}\right)(\cos(\omega t) + \sin(\omega t))\right. \\ & \left. + \sin\left(\frac{2h}{\delta}\right)(-\cos(\omega t) + \sin(\omega t))\right),\end{aligned} \tag{32}$$

$$M_{dis}{}^{\dagger} = \frac{\pi\Omega_0\sqrt{\omega\rho\eta}R^4\sin(\omega t)}{\sqrt{2}} \cdot \frac{\sinh\left(\frac{2h}{\delta}\right) + \sin\left(\frac{2h}{\delta}\right)}{\cosh\left(\frac{2h}{\delta}\right) - \cos\left(\frac{2h}{\delta}\right)}, \tag{33}$$

$$k^{\dagger} = \frac{\pi\sqrt{\omega\rho\eta}R^4}{\sqrt{2}} \cdot \frac{\sinh\left(\frac{2h}{\delta}\right) + \sin\left(\frac{2h}{\delta}\right)}{\cosh\left(\frac{2h}{\delta}\right) - \cos\left(\frac{2h}{\delta}\right)}, \tag{34}$$

$$k_{eff}{}^{\dagger} = \sqrt{2\omega\rho\eta}R^4 \cdot \frac{\sinh\left(\frac{2h}{\delta}\right) + \sin\left(\frac{2h}{\delta}\right)}{\cosh\left(\frac{2h}{\delta}\right) - \cos\left(\frac{2h}{\delta}\right)}, \tag{35}$$

$$\varepsilon^{\dagger} = \frac{\pi{\Omega_0}^2\sqrt{\omega\rho\eta}R^4\sin^2(\omega t)}{\sqrt{2}} \cdot \frac{\sinh\left(\frac{2h}{\delta}\right) + \sin\left(\frac{2h}{\delta}\right)}{\cosh\left(\frac{2h}{\delta}\right) - \cos\left(\frac{2h}{\delta}\right)}, \tag{36}$$

$$\varepsilon_{eff}{}^{\dagger} = \frac{\pi{\Omega_0}^2\sqrt{\omega\rho\eta}R^4}{2\sqrt{2}} \cdot \frac{\sinh\left(\frac{2h}{\delta}\right) + \sin\left(\frac{2h}{\delta}\right)}{\cosh\left(\frac{2h}{\delta}\right) - \cos\left(\frac{2h}{\delta}\right)}. \tag{37}$$

As we would expect, in the limit $h<<\delta$ these relationships reduce exactly to those derived for the example of a torsionally oscillating disc in an infinite volume of fluid. Figure 1.6 shows this limiting behaviour of the effective damping coefficient. As in our case $\delta_{max} = 0.475$ mm and $h = 4.5$ mm, it is evident that we can use the expressions derived in the first example.

To compare with experimental data, an expression for the relaxation time, τ derived from the solution to the equation of motion of a linearly damped harmonic torsional oscillator, will be used:

$$\tau = \frac{2I}{k} = \frac{4I}{\pi\, k_{eff}}. \tag{38}$$

where $I = \frac{1}{2}mR^2$ is the moment of inertia of the disc, m its mass and R its radius. One of the assumptions used in all the calculations is that the initial deflection is small; due to that, the inertial term of the Navier-Stokes equation can be neglected. The derived results thus apply only to the situation where laminar flow takes place around the disc. In the event that the flow is turbulent, we expect the frictional forces and energy dissipation to exceed the values derived above, and the damping coefficients k and k_{eff} will become functions of the angular velocity amplitude. Our goal will be, among others, to identify the critical values of relevant quantities at which this occurs.

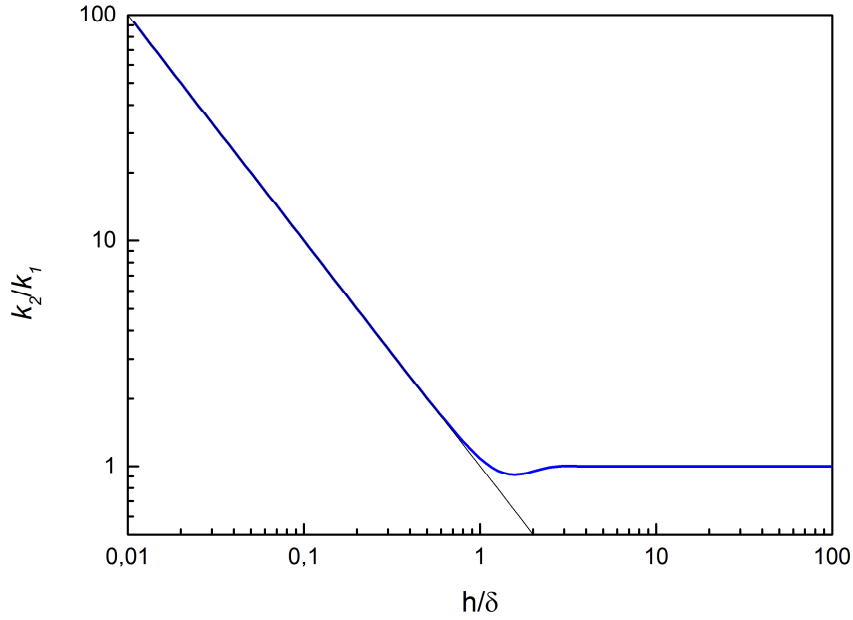

Fig. 1.6: Ratio of the damping coefficient calculated for the disc between two plates to the damping coefficient obtained for a disc in an infinite volume of fluid plotted against the distance of the disc from the plates divided by the viscous penetration depth. If the disc is moved away from the plates by at least five penetration depths, the two cases become essentially equivalent, whilst in the limit of low h/δ, the ratio of the damping coefficients scales inversely proportional to this parameter, as illustrated by the thin straight line.

To provide a means to handle non-linear drag forces arising if turbulence is present, we do the following. In analogy with the situation where a body moves linearly in a fluid experiencing a non-linear drag force $F = \frac{1}{2} C_D' \rho A' U^2$, where C_D' is the dimensionless drag coefficient, A' the cross-sectional area and U the velocity, it can be shown by evaluating a similar integral as we used to calculate the moment of drag forces, one may define a drag coefficient for the torsional motion of the disc:

$$C_D = \frac{2\, k_{eff}}{\rho R^5 \Omega_0} = \frac{4}{Re_\delta}, \tag{39}$$

where R is the radius of the disc. This drag coefficient is expected to follow a $1/\Omega_0$ dependence in laminar flow, which starts to change gradually at the critical angular velocity to become a constant in developed turbulence.

Finally, in the case of flow around the oscillator in superfluid helium, it is necessary to replace all the densities and viscosities by the values for the normal component (noting that the kinematic viscosity of the normal component $\nu_N = \eta/\rho_N$),

because unless quantized vortices are created and quantum turbulence occurs, the superfluid component will either stay at rest or exhibit potential flow and will not contribute to the dissipative forces acting on the disc. For the drag coefficient in superfluid helium, we will use both varieties with the density ρ replaced by ρ_N or ρ_S as needed: $C_{DN} = 2k_{eff}/\rho_N A\Omega_0$ and $C_{DS} = 2k_{eff}/\rho_S A\Omega_0$.

In the next section, a description of the experimental setup and the measurement technique will be given.

2 Experimental Setup

The experiment was conducted in a glass cryostat consisting of two Dewar flasks. The exterior one is opened outwards and serves for precooling by liquid nitrogen. This dewar is silver-plated in its vacuum space to reduce radiative heat transfer into the inner flask. In the layer of silver there are two vertical visors of a width of about 3 cm along the entire height of the cryostat. As we employed video recording to measure the motion of the disc, it was necessary to cover the visors with black paper leaving only a 1 cm high viewport at the level of the disc.

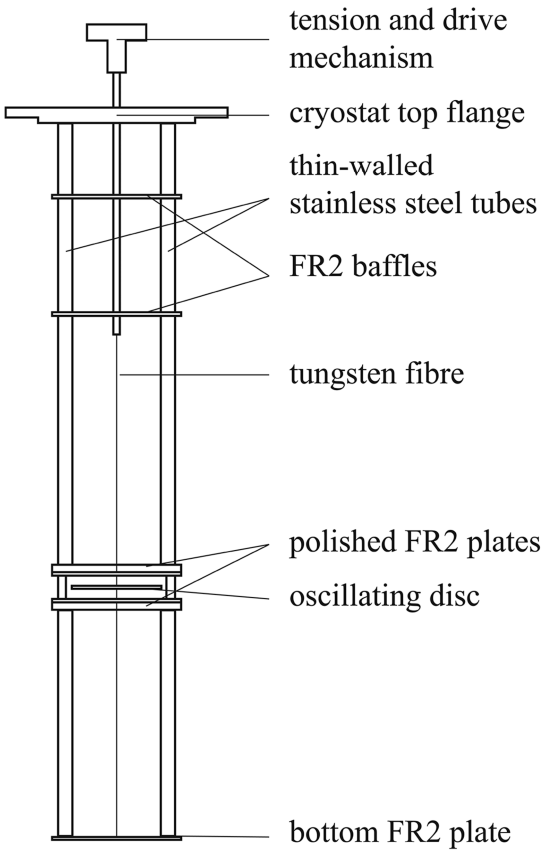

Fig. 2.1: A schematic sketch of the cryostat Insert housing the oscillating disc suspended on the tungsten torsional fibre.

Around the inner vessel, six white LEDs were placed at the level of the disc. The LEDs were distributed evenly around the circumference in such a way as to avoid the line-of-sight of the video camera. White paper was put around the inner dewar to provide soft diffuse lighting and a uniform image background.

The experimental setup, shown in figure 2.1, was placed in the inner dewar, which can be filled with liquid helium and pumped on by a Roots pump to reduce the saturated vapour pressure down to about 1.5 Torr corresponding to temperatures just above 1.3 K.

The top flange of the cryostat had three ports connecting to the interior of the helium vessel. Two of them were used for transferring helium and measuring the pressure, which was later used to infer the temperature from the saturated vapour pressure dependence as given by the HEPAK software [19; 20]. Through the central port, a small assembly consisting of a pipe with a threaded rod, a top nut, a counter nut, and a ball bearing was connected to the interior of the inner vessel. Inside it was connected to a thin-walled stainless steel tube that extended downwards and at its lower end held the tungsten wire, on which the disc was suspended.

The assembly at the top flange was used to apply tension to the tungsten wire as needed and also to rotate the disc freely without changing the tension of the wire.

A support construction was fixed to the bottom side of the cryostat flange. The structure consisted of four thin-walled stainless steel tubes held together by brass rings and FR2 baffles. It was made of two parts, which had the oscillating disc in between them and were connected by three cylindrical brass spacers 10 mm in height. The upper part of the structure contained several baffles used to guide the tube connecting the tungsten wire to the top flange assembly and to reduce the heat leak. At the bottom of this part, a brass ring and a FR2 plate with polished surface was fixed, which provided the upper boundary to the volume of helium in the immediate vicinity of the disc.

The lower part of the structure was almost a mirror image of the top part (around the plane of the disc), except that it was terminated at the bottom by another FR2 plate to which the other end of the tungsten wire was fixed. Below the lowest plate, a 50 Ω heater was placed. It was used to evaporate any helium left after the experiment has finished.

The torsional oscillator itself consisted of a 0.05 mm tungsten wire 32 cm long and the disc fixed to the wire in the middle of its length using a thin 0.8 mm brass capillary and Stycast 1266. The disc itself was made of Plexiglas of 1 mm thickness and had a diameter of 50 mm. When the wire was pulled taut, the disc was positioned approximately midway between the two polished FR2 plates, i.e., roughly 4.5 mm away from either plate. Sixteen black marks were made evenly around the circumference of the disc, which would later be used to determine the deflection and angular velocity of the disc from the recorded sequences.

The motion of the disc was recorded with a Canon EOS 600D digital camera fitted with a Canon EF-S 18-135 mm f / 1:3.5 - 5.6 IS lens. The recording was acquired in 1280x720 resolution at the framerate of 50 fps.

3 Experimental Results

3.1 Data Processing

Our raw data was in the form of video recordings of the motion of the disc during the experiments. Because the marks on the disc were relatively small compared to the entire field of view, with relatively low contrast to the not-entirely-uniform background, standard motion tracking software could not be used to process the videos. Hence, fairly complex post-processing was required to extract quantitative and interpretable data.

Firstly, it was necessary crop the recorded video, cutting away the plates above and below the disc, as well as the cryostat shield and leaving only the area of interest in the immediate vicinity of the disc. The video was then split into individual frames, de-interlacing them in the process, which meant that only pixels recorded at exactly the same time were kept. To achieve both of these goals, the commercial program VideoMach was used.

The obtained images were further processed in Adobe Photoshop CS2, where in a series of ten to fifteen steps, the colour images were converted to monochromatic bitmaps. These involved filtering the image in various ways, using the colour information in such a way and enhancing the low contrast of the marks so that they would become black contiguous spots on white background. This process included blurring filters and the removal of small specks, which led to the fact that not all the captured marks were reproduced in each individual image, as the settings of all the filters and modifications were kept the same for each of the roughly 10,000 to 35,000 frames of a given recording.

The resulting monochromatic bitmaps were used as input for a home-made program created in the NI LabView environment. In each image, the program localised the black areas evaluating their size and centre of mass. It then assigned individual dots between consecutive images to each other (making special arrangements for those not reproduced in some of the bitmaps) and calculated the average displacement between the two frames in pixels. This basically gave us a value of the circumference velocity in pixels per frame. At the same time, the software controlled the physical meaningfulness of the emerging pattern of motion, as it was known that the disc would exhibit damped oscillations.

The program output a text file containing records of the size, the position of each dot in each frame and the displacement between frames.

The velocities obtained in the previous steps were then inserted into the Origin processing and graphing software. Here they were converted from pixels per frame to radians per second assuming that the optical effects due to several curved glass plates are negligible, as only the central region of the field of view was kept for processing, and the results were plotted against time. Based on the graphs, irrelevant data were removed; the beginning of each signal, where the disc had not yet been spun, and the signal end, where all meaningful information was lost in the noise. The remaining data were smoothed before further processing to improve accuracy. We used the Savitzky-Golay algorithm for curves dominated by random noise, or the low pass FFT filter with the cutoff frequency of 1 Hz for curves distorted by weak oscillations at other frequencies, such as the low amplitude (< 1 mm) pendular motion of the suspended disc, or generally any noise exhibiting periodic behaviour. Each smoothed signal was carefully checked against the original to avoid processing artifacts.

The smoothed data were again exported as a text file and processed in a second program created in LabView. This program sought all extrema of the signal and returned their values and the times when they occurred, with the intent to extract the envelope of the decaying oscillating signal. If needed, additional filtering algorithms were employed before the extrema were extracted. The values and times of the extrema were found from a parabolic fit to the neighbourhood of a local discreet maximum or minimum in the signal.

The resulting data were further processed and plotted in Origin. Comments for this process and its results along with their interpretation will be given in the following section.

3.2 Interpretation

Before the actual measurement, preliminary tests were carried out at room temperature (in air at 1 bar and in vacuum) and near liquid nitrogen temperature in vacuum. The time evolutions of the angular velocities during tests are plotted in figure 3.1. We see that the damping of the oscillator is affected both by the change in temperature and pressure. This was an encouraging result, meaning that the disc should be sensitive to dissipative forces from the surrounding fluid, as well as that its intrinsic energy dissipation (mainly within the torsional fibre and connections) will be negligible at helium temperatures compared to both laminar and turbulent drag forces. Note that the decay time in vacuum near LN_2 temperature is already over 400 s, much larger than the signals subsequently measured, even in superfluid helium at the lowest temperatures. Moreover, the intrinsic damping, which is mainly due to the motion of vacancies and dislocations in the fibre, is expected to drop even further between LN_2 and LHe temperatures.

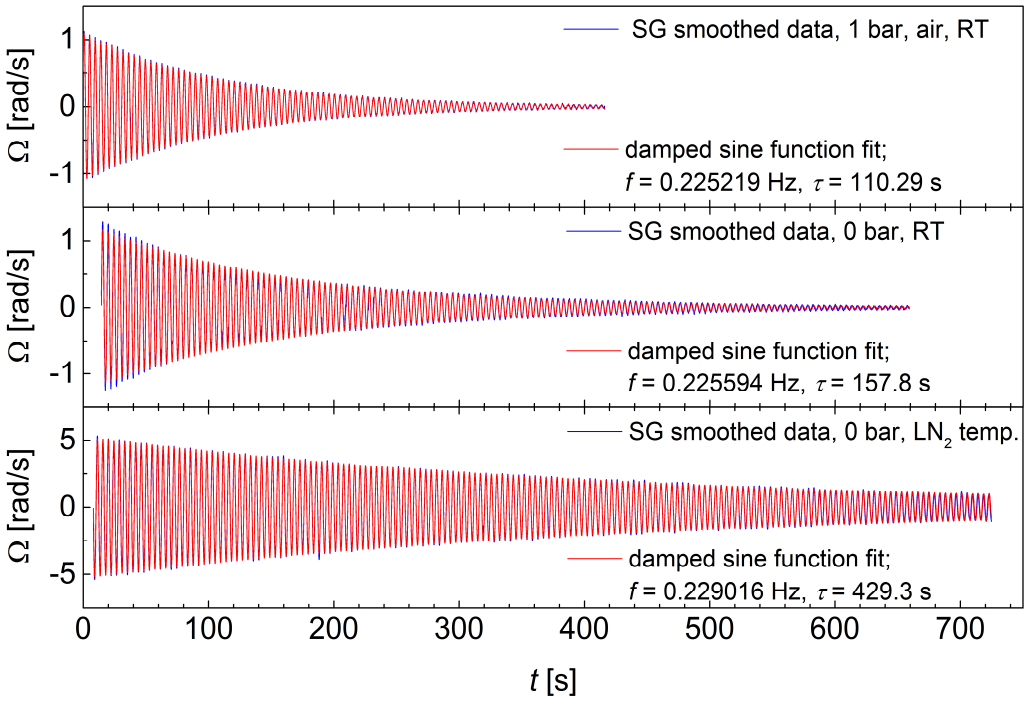

Fig. 3.1: Time traces of the signals of angular velocity recorded during test measurements at room temperature and liquid nitrogen temperature, as indicated. The decays are perfectly described by a damped sine function, i.e., no non-linearities are observed in this case.

During the tests, we ran into several problems. We found that it was necessary to improve the uniformity of the background. This was done by using white paper located on the outer side of the helium vessel. The exterior lighting reflecting on the glass of the cryostat made it very difficult to record usable videos. For the main measurements, we solved this by installing LEDs into the liquid nitrogen space of the cryostat, which significantly improved the lighting conditions during filming. Also, the bubbles caused by evaporation in the nitrogen tank had an adverse impact on the recording quality since they crossed the field of view, distorting the image. After initial unsuccessful attempts to prevent bubbles from passing through this area by placing obstacles below the field of view, we decided to try a different approach by creating a horseshoe-shaped bubble trap instead, which maintained the level of liquid nitrogen below the field of view.

For these tests, the recordings were acquired at a frame rate of 25 fps with a resolution of 1920x1080. However, during processing, we found that the main measurement would require a frame rate of at least 50 fps. The camera was only capable of filming at this rate with a maximum resolution of 1280x720, but this was sufficient for our needs.

Measurements were only performed in the superfluid phase He II because measurements in He I would be very difficult due bubbles being formed throughout the entire volume of the liquid. Thus, our measurements began just below the lambda point and subsequently by reducing the vapour pressure the liquid temperature was lowered to selected values. During the measurements, it was necessary to correct the pumping rate such that the pressure in the vessel is as constant as possible. An example of the measured signal that was acquired at the lowest temperature that we achieved, 1.37 K, is plotted in figure 3.2. Along with the temporal evolution of the angular velocity, we also plot the logarithms of the signal maxima that will be used in further processing.

From the lower plot, we clearly see the transition to the non-linear resistive force, indicating the onset of non-laminar flow at the highest amplitudes and the presence of some form of turbulence. By comparing figures 3.1 and 3.2, it can be seen that the oscillation amplitude in superfluid helium decays faster ($\tau \approx 200$ s) than in vacuum, even at liquid nitrogen temperature. Taking into account our experience with other types of resonators, such as the tuning forks, we estimate

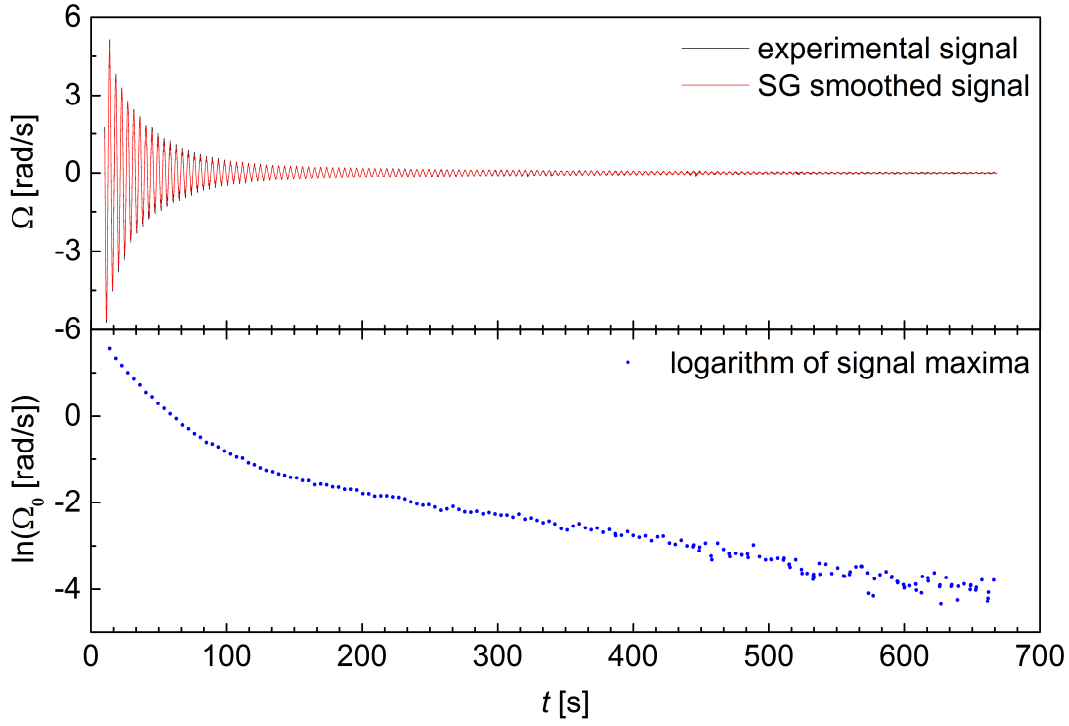

Fig. 3.2: (top) An example of a signal of angular velocity recorded in superfluid helium. The observed damping significantly exceeds that measured in vacuum at liquid nitrogen temperature (figure 3.1). (bottom) Logarithms of the maxima of the signal shown in the upper panel. Plain exponential decay characteristic of laminar flow is seen as a straight line dependence at late times, while the changes at around 100 s indicate instability in the flow.

that the damping of the fibre at helium temperatures (in vacuum) would be roughly an order of magnitude lower than at nitrogen temperature, which justifies neglecting the intrinsic dissipation of the fibre in further processing. Note that it would be difficult to measure the vacuum dissipation rate at helium temperature directly, as the tungsten wire would not be properly thermalised and a temperature profile ranging from room temperature (at the top flange) to LHe temperature would develop along its length.

In figure 3.3, we show the logarithms of signal maxima for each measurement at different temperatures. The measurements are divided into groups according to the temperature and the behaviour of the signal.

Notice how the logarithms of the signal maxima behave at various temperatures. For almost all measurements (exceptions will be discussed below), the slope of the linear part of the curve varies proportionally with temperature. This is because the dissipative forces in the laminar part originate in the normal component

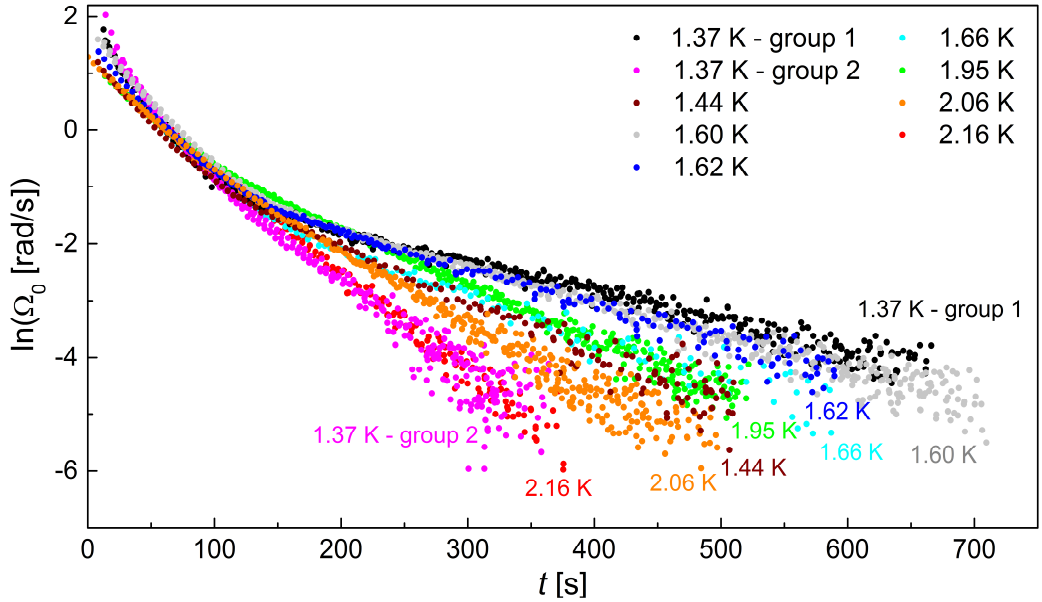

Fig. 3.3: Logarithms of the amplitude of angular velocity as a function of time at various temperatures. The slope of the linear part should decrease with decreasing temperature, as does the drag force due to the normal component. Two of the data sets (1.37 K – group 2 and 1.44 K) do not follow this tendency and have been removed from further processing as they are affected by the liquid helium level dropping near the upper plate above the disc (see text).

and thus have to scale with its density according to equation (26), resulting in the smallest slope for the lowest temperature, etc. This is not true for measurements listed as "1.44 K" and "1.37 K – group 2", because while filming these, the superfluid helium level was already very close to the disc and hence we have no knowledge of the temperature of the filament above it. Therefore, these measurements were removed from further analysis.

Since we are mainly interested in the analysis of the non-linear part of the data for each temperature, the laminar part of the graph was fitted by a straight line, which was then withdrawn from the logarithms of the signal maxima. The area of fitting was selected manually with care taken to avoid influence from the non-laminar part as well as from the noisy signal at late times (low amplitudes). This process is illustrated, for example, in the data for 1.37 K shown in figure 3.4. In Table 3.1 we list the fit constants and relaxation times calculated in this way for all available temperatures.

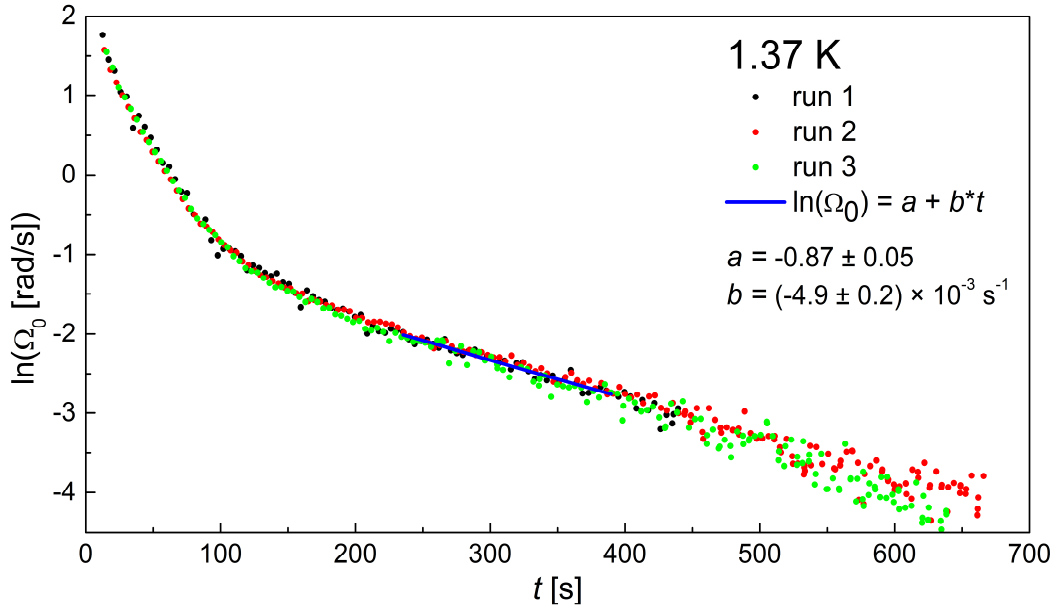

Fig. 3.4: An example of fitting the linear part of the decay by a straight line. Care was taken to avoid the fit being distorted by the noisy part at the lowest amplitudes and by the onset of instability observed at early times.

Tab. 3.1: Values of the fit parameters a and b for various temperatures together with the relaxation time $\tau = -1/b$.

T [K]	a	b [× 10^{-3} s^{-1}]	τ [s]
1.37	-0.87 ± 0.05	-4.9 ± 0.2	203 ± 6
1.60	-0.49 ± 0.03	-6.4 ± 0.1	156 ± 2
1.62	-0.50 ± 0.03	-6.5 ± 0.1	153 ± 2
1.66	-0.61 ± 0.06	-7.6 ± 0.2	131 ± 4
1.95	0.26 ± 0.02	-10.0 ± 0.1	100 ± 1
2.06	0.43 ± 0.03	-12.8 ± 0.2	78 ± 1
2.16	1.16 ± 0.03	-18.4 ± 0.2	54 ± 1

In the upper panel of figure 3.5, we plot the logarithms of the signal maxima (after subtracting their laminar contribution) against the amplitude of the angular velocity for all temperatures. The change of the slope of the non-laminar part with temperature suggests that the non-linear force may originate from the superfluid component as its magnitude might scale approximately with the density of the superfluid component. In the lower panel, we plot these curves normalised by the density of the superfluid component. The almost identical slopes of the non-laminar parts confirm our previous suggestion that the drag force in this regime scales with the density of the superfluid component, at least

for temperatures between 1.37 K and 1.95 K. This demonstrates that in the superfluid component, a significant amount of quantized vortices are present, since without them, the superfluid component has no means whatsoever to act dissipatively on the oscillating disc.

At 2.16 K, the normal fluid fraction is over 90% and it dominates the fluid's dynamics. Here, we see no hints of a non-linear dissipative force at all, except perhaps for the very highest angular velocities above 2 rad/s. This corresponds to a value of $Re_{N\delta} = \Omega_0 R\sqrt{2\,\rho_N/\eta\,\omega} \cong 450$, which was only reached in our experiments at temperatures of 2.16 K, 2.06 K, and barely reached at 1.95 K. This means that at lower temperatures, the normal component could not become turbulent of its own accord in the examined range of angular velocities, without the influence of the superfluid component.

This would, together with the scaling of the non-linear force at lower temperatures, seem to imply that under the given conditions the normal component is most likely still laminar. If this is shown to be true, it would represent an important result in the sense that it would provide an answer to one of the long-standing questions in two-fluid hydrodynamics, giving a direct proof of the existence of a situation where the superfluid component contains enough quantized vortices to induce a measurable non-linear drag force, while at the same time the normal component maintains laminar flow. However, before jumping to such conclusions, more careful analysis is required.

From figure 3.5, we have also estimated the critical angular velocity for the decay of quantized vortices in the superfluid component. That is also the reason why we use the angular velocity as the independent variable rather than the dimensionless characteristic numbers, which are meaningful only for the normal component. As an example of the estimation of the critical angular velocity, we show figure 3.6. We should note that this estimation is subjective and prone to significant errors, perhaps up to a factor of 2. However, given the noise levels in the laminar part, we believe that the precision could not be increased significantly if more quantitative methods were used.

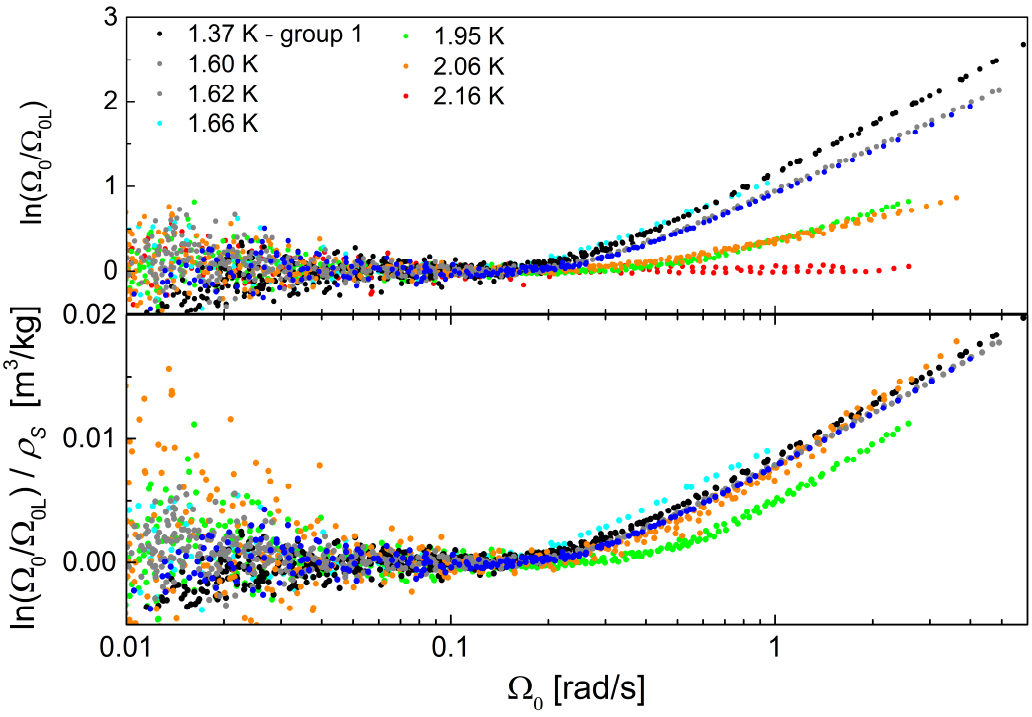

Fig. 3.5: (top) Logarithm of the angular velocity amplitude with the linear part withdrawn (as shown in figure 3.4) plotted against the angular velocity amplitude. At 2.16 K no signs of non-linear dissipation are present except at the very highest angular velocities. The non-linear drag (proportional to the slope of the dependence) seems to increase with decreasing temperature. (bottom) The same quantity as above divided by the superfluid component density, ρ_S. The non-linear drag has collapsed to the same slope of the dependence for all temperatures (except for the data taken at 2.06 K), showing that it is proportional to ρ_S and thus originates from the superfluid component.

In figure 3.7, we plot the time derivative of the logarithms of the signal maxima, which is linked to the theoretical quantities by: $d\Omega_0/dt = -1/\tau$, against the angular velocity amplitude and the arrow marks the critical velocity determined according to the procedure outlined above. Looking closely at the dependence of the time derivative above the critical velocity, a question immediately arises of whether only one critical velocity has been measured. These data would be readily interpreted if we assumed a region dominated by quasi-laminar flow (constant value of the time derivative) in the vicinity of 1 rad/s and a second transition near 2 rad/s. This second transition has only been observed reliably at the lowest temperature, 1.37 K with only a hint of similar occurrence at temperatures near 1.6 K.

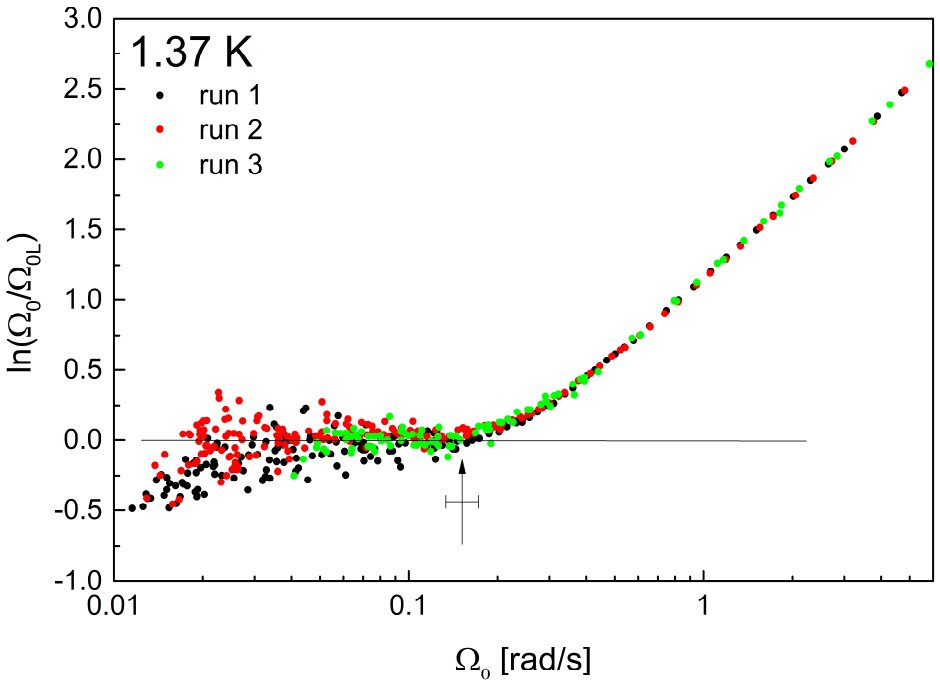

Fig. 3.6: An example of the determination of the critical angular velocity for the temperature 1.37 K. The critical velocity (black arrow with error bar) is estimated to be located at the point where the dependence first noticeably diverges from the horizontal line passing through zero on the y axis. We estimate the uncertainty of such a critical value determined from this type of graph to be below 20%.

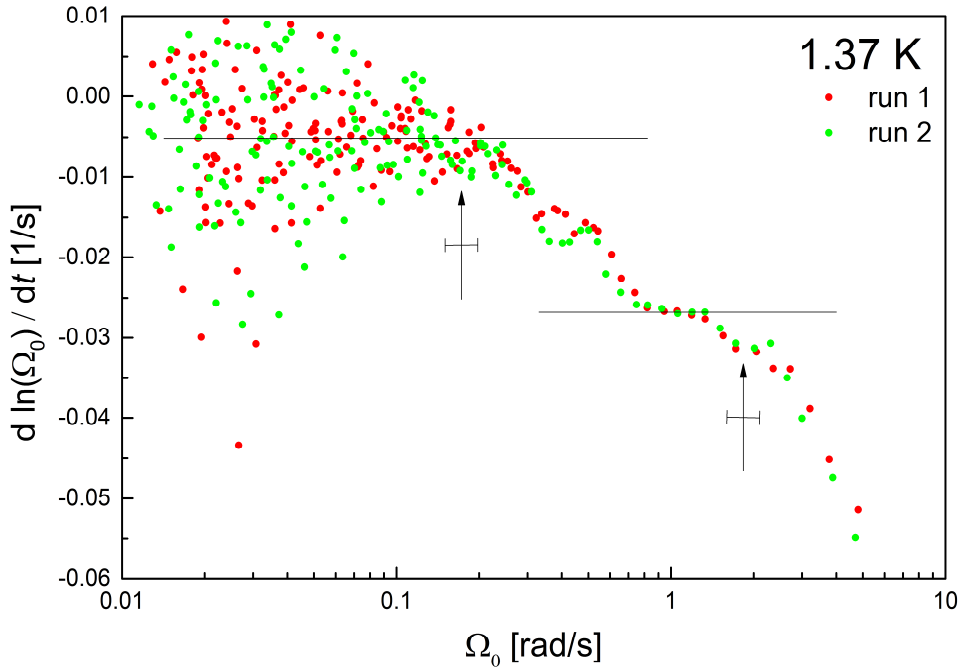

Fig. 3.7: The time derivative of the logarithm of the amplitude of the angular velocity plotted against the angular velocity amplitude for the temperature 1.37 K. The critical velocity, determined as explained in the text, is shown by the left black arrow and error bar, but we also see an indication of a second critical angular velocity between 1 and 2 rad/s. The solid lines are guides for the eye.

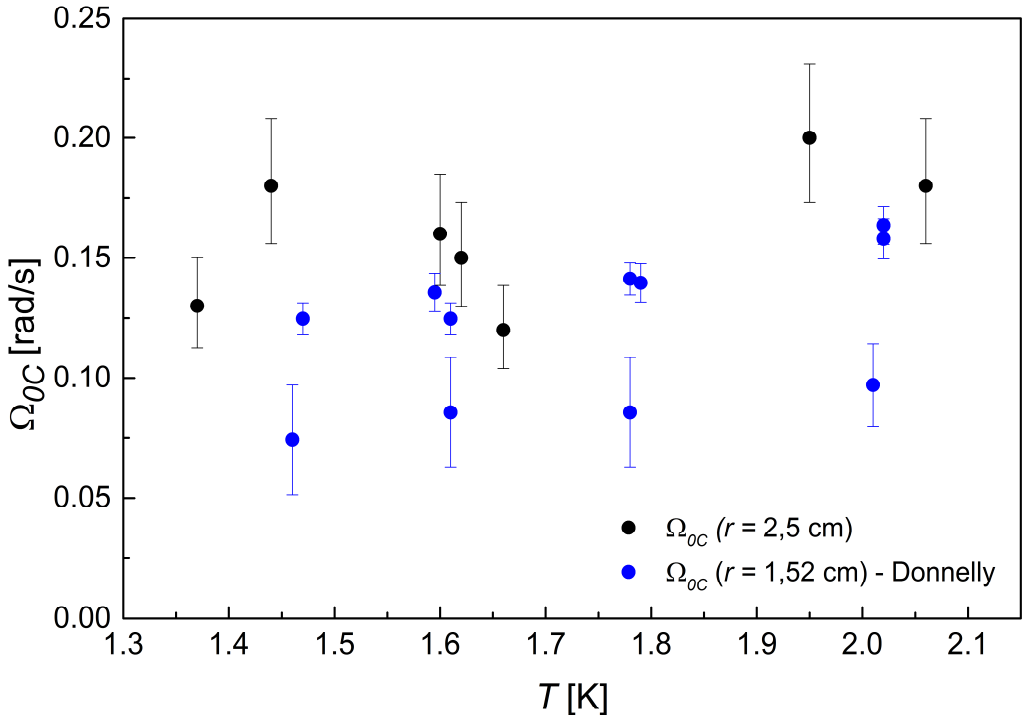

Fig. 3.8: The (lower) critical velocity plotted against temperature and for comparison, the results of Donnelly and Hollis Hallet [7]. Despite the uncertainties and the scatter of the data, it seems that in both cases the data display only a weak temperature dependence and that they are in mutual agreement.

As we can see in figure 3.8, our values of the (lower) critical angular velocity seem to correspond to the values obtained by Donnelly and Hollis Hallett [7]. If we assumed that it is the speed at the circumference which matters instead, the agreement would be worse because of the different radii of the discs used. Given also the scatter of the data, no strong conclusions about the observed critical angular velocities can be made at the moment, except perhaps that in both cases the same type of instability has been observed and that only a weak temperature dependence is found, which again supports the idea of an instability in the superfluid component, as the viscosity of helium and the density of the normal fluid both change dramatically with temperature, affecting the relevant flow parameters such as the Reynolds numbers Re or Re_δ.

However, with the current knowledge at our disposal, our work leads to a somewhat different interpretation of the results than that given in ref. [7], as more information about the dissipative forces could be extracted from the digitally recorded data. Additionally, in their experiments with the torsionally oscillating disc,

Donnelly and Hollis Hallett never seemed to reach the second critical angular velocity [7], although they have seen it with other devices such as a torsionally oscillating sphere. From our results, it follows that at angular velocities higher than the first critical value and less than the second, quantized vortices are formed in the superfluid component causing a non-linear dissipative force. We shall now examine the dissipative forces in more detail and compare them to the theoretical predictions.

In the two following figures, the experiments are compared with the theory of laminar flow around the oscillating disc. In figure 3.9 and 3.10, we plot the experimental and theoretical values of the effective damping coefficient k_{eff} and the effective energy dissipation ε_{eff} for three different temperatures: 1.37 K, 1.95 K and 2.16 K against the angular velocity, respectively.

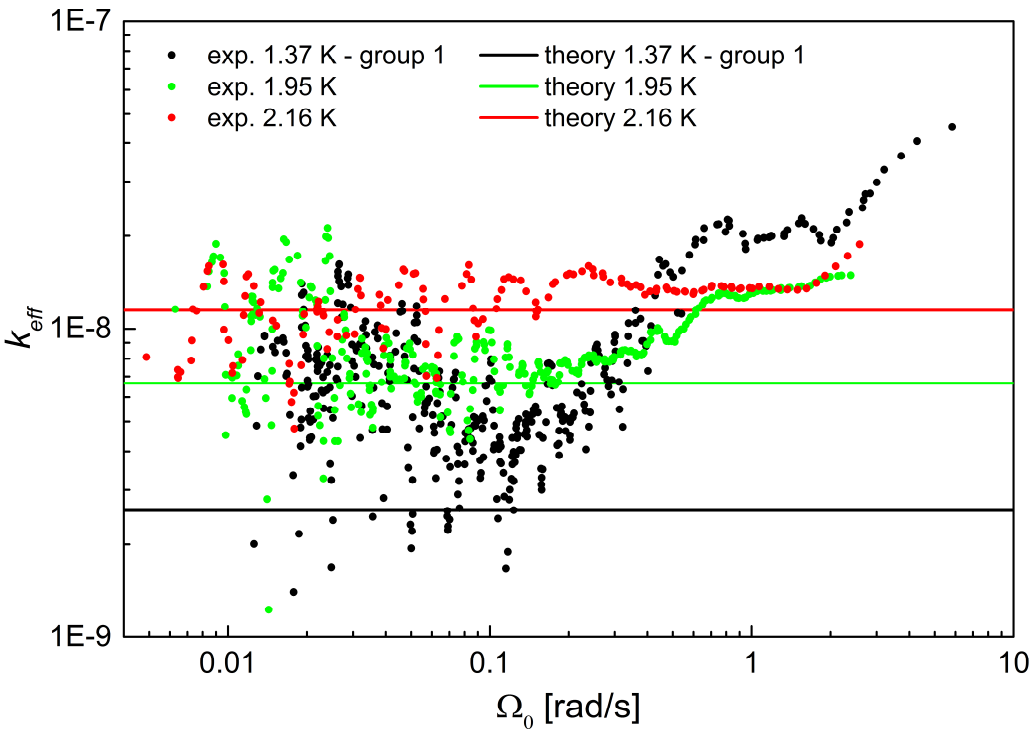

Fig. 3.9: Comparison of the experimental effective damping coefficients with the theory for laminar flow of the normal component at the indicated temperatures. The theoretical values always seem to be lower than the experimental ones, the reasons for which are given in the text. In this plot, we also observe the two critical velocities in the data taken at 1.37 K.

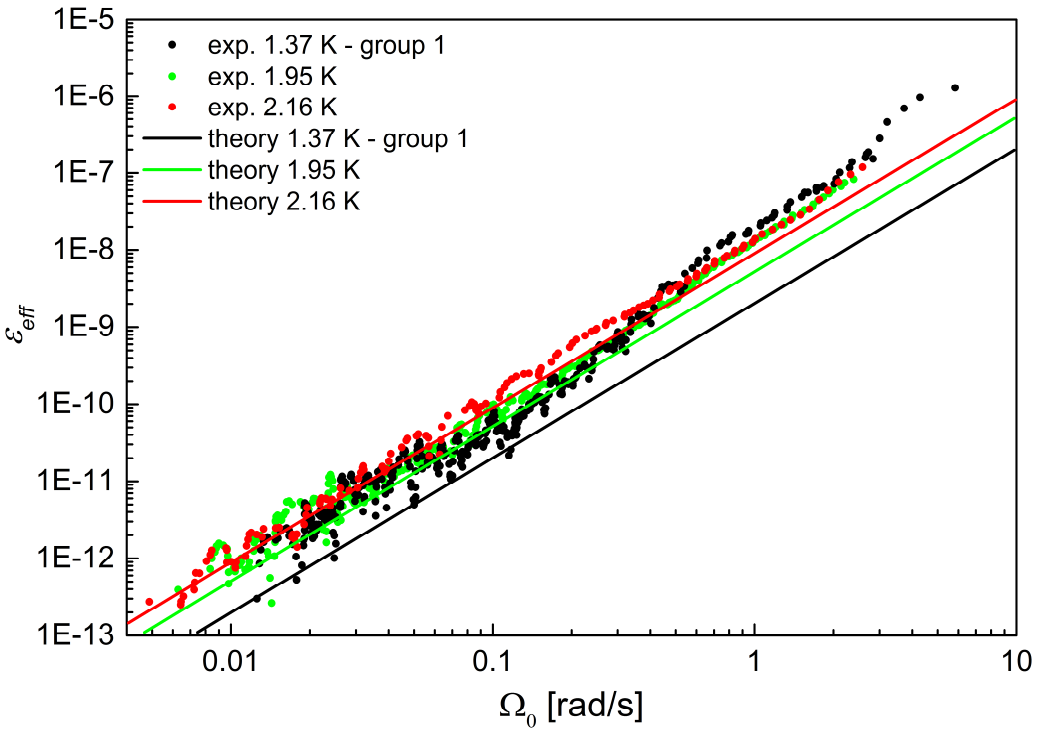

Fig. 3.10: The effective energy dissipation rate plotted against the angular velocity amplitude for the indicated temperatures and for comparison, the corresponding predicted dependencies. The rates are sufficiently low to discount any significant heating of the superfluid in the vicinity of the oscillating disc.

From both figures, it can be seen that the theory predicts a lower drag force from the surrounding fluid than we measured. This is hardly surprising since the theoretical calculations do not consider the presence of the cylindrical cryostat wall. Moreover, the disc did not exhibit perfect torsional motion during the experiment, as it was not completely perpendicular to its suspension fibre. Also, it would have experienced small sideways vibrations as a result of the cryostat being connected to the vibrating Roots pump or when the disc was spun. Furthermore, the disc also has a rough surface; in fact the surface roughness is likely to be on scales comparable to the viscous penetration depth, which would increase the drag noticeably. Theoretical values can be calculated from the relations (28) and (30) as the viscous penetration depth was almost ten times less than the distance of the plates from the disc. In both plots, we can also see the transition from the linear damping force.

To further disentangle the contributions of the two components of He II and formulate a scenario for the behaviour of superfluid helium around a torsionally

oscillating disc, we will examine the drag coefficients defined for the torsional motion of the disc in Section 1.3.

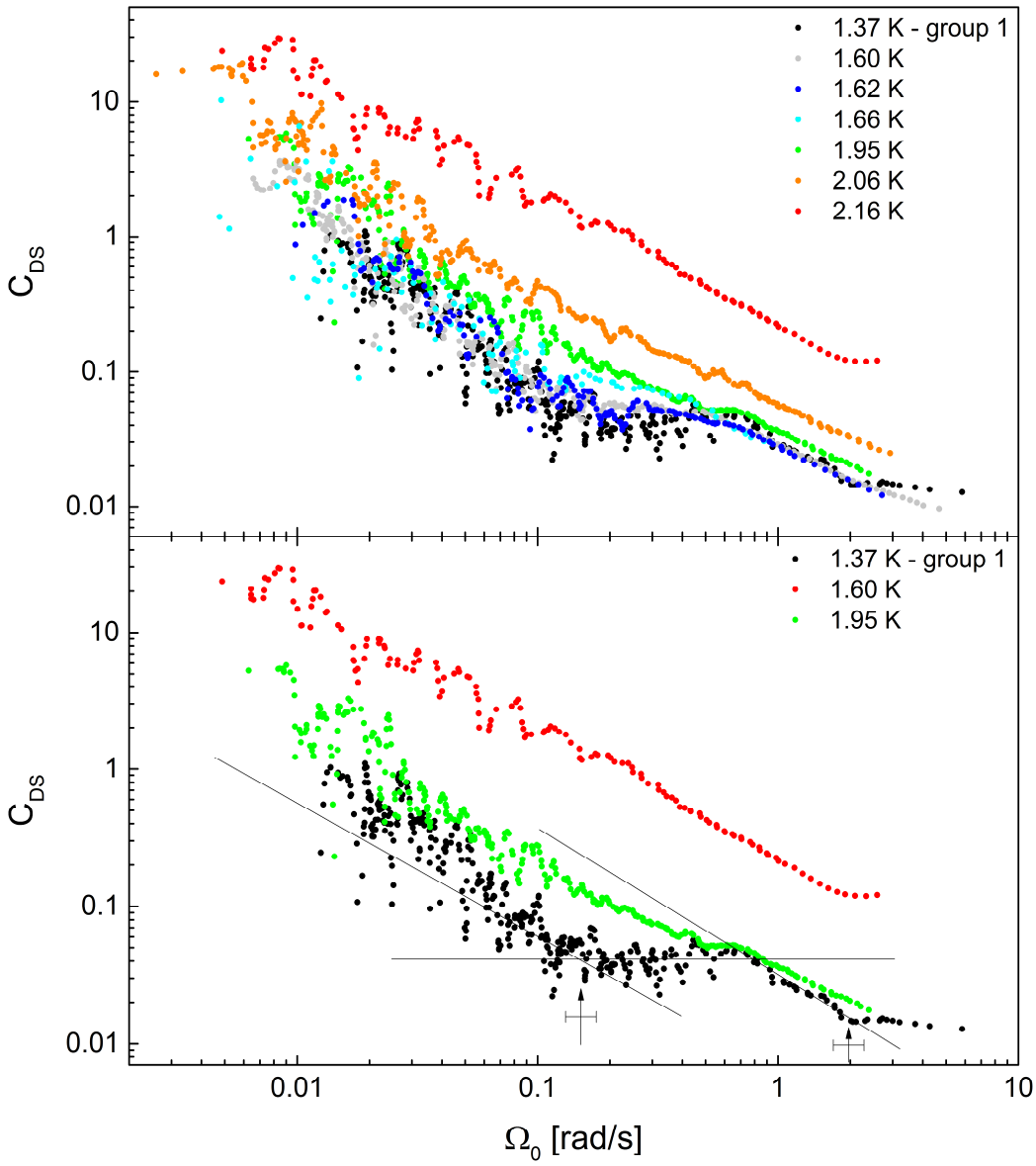

Fig. 3.11: The drag coefficient for the superfluid component plotted against the angular velocity amplitude for all the analysed temperatures (top) and for selected temperatures, as indicated, for clarity (bottom). The solid lines are guides for the eye and represent either inverse proportionality dependences or a constant value of the plotted drag coefficient. Two regions of quasi-laminar flow are clearly identified in the data taken at 1.37 K. Furthermore, the behaviour at angular velocities around 1 rad/s is almost identical for all temperatures below 2 K. Needless to say, the drag coefficient for the superfluid component is not a very meaningful quantity for interpreting the data taken at 2.16 K, as the fractional density of the superfluid component is very low – only about 7%. We plot this dependence for comparison, nonetheless.

In figure 3.11, the dependence of the superfluid drag coefficient is plotted against the angular velocity amplitude and again, we see that the data from the lowest temperatures collapse to a single dependence, once the (lower) critical angular velocity is exceeded. This is in agreement with our previous findings that the first non-linear damping force is due to the superfluid component. On the other hand, the laminar part at the lowest values of angular velocity does not collapse, as it is the normal fluid component that is responsible for the dissipative force.

Furthermore, from this graph (selected data isolated in the lower panel) we clearly see that at the lowest temperature, there are two regions that exhibit laminar-like behaviour, which is recognized as the functional dependence $C_{DS} \propto 1/\Omega_0$, in contrast to turbulent flow that would be characterised by $C_{DS} \approx const$. This is essential for our understanding of the processes occurring near the critical angular velocity, as it shows that after the lower critical angular velocity is exceeded, He II behaves as if it were turbulent in a limited range of Ω_0, where we already know that the non-linear drag arises from the superfluid component, but then again starts to exhibit quasi-laminar flow, despite the fact that there is a significant amount of quantized vortices already present in the superfluid component. All of this is best seen at the temperature 1.37 K where the fractional density of the superfluid component is highest and thus, its contribution towards the drag forces is the most significant.

Figure 3.12, where the normal component drag coefficient is plotted against the angular velocity is perhaps only illustrative, but it still shows the dissipative force beginning to rise above the laminar contribution at approximately the same value as the critical angular velocity determined earlier.

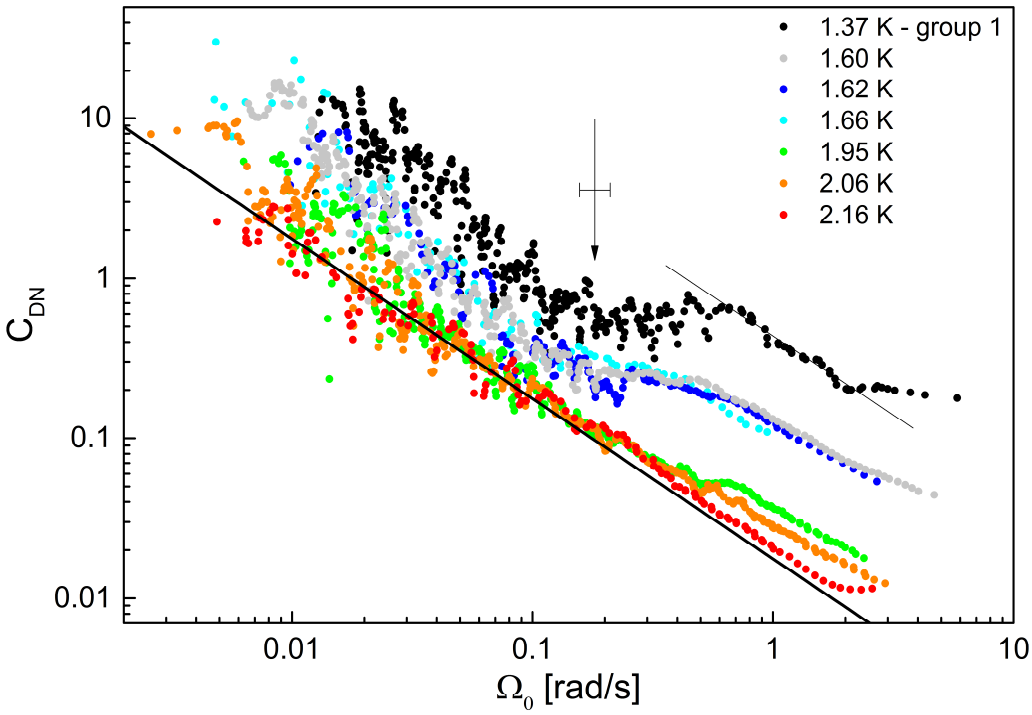

Fig. 3.12: The drag coefficient for the normal component plotted against the angular velocity amplitude for all the analysed temperatures. While no portion of the data can be collapsed in this type of plot, it shows quite clearly the critical angular velocity and the quasi-viscous behaviour around 1 rad/s as indicated for the data taken at 1.37 K (black arrow with error bar; upper black line, respectively). The lower black line corresponds to equation (39) for the temperature 2.16 K.

It becomes more interesting if compared with figure 3.13, where the drag coefficient for the normal component is plotted against the Reynolds number calculated using the viscous penetration depth as the characteristic length scale. From the collapse of the laminar part, one can see that the viscous drag of the normal component does indeed scale as predicted and that we are really operating the disc in the "high frequency limit", despite its very low natural frequency of about 0.22 Hz. If only the normal component had been responsible for the measured drag forces here, all dependences should have collapsed to a single line, similar to the data taken at 2.16 K that are indeed dominated by the action of the normal component (over 90% fractional density). Thus, any significant departure from the baseline approximately given by this measurement must again only be due to the superfluid component.

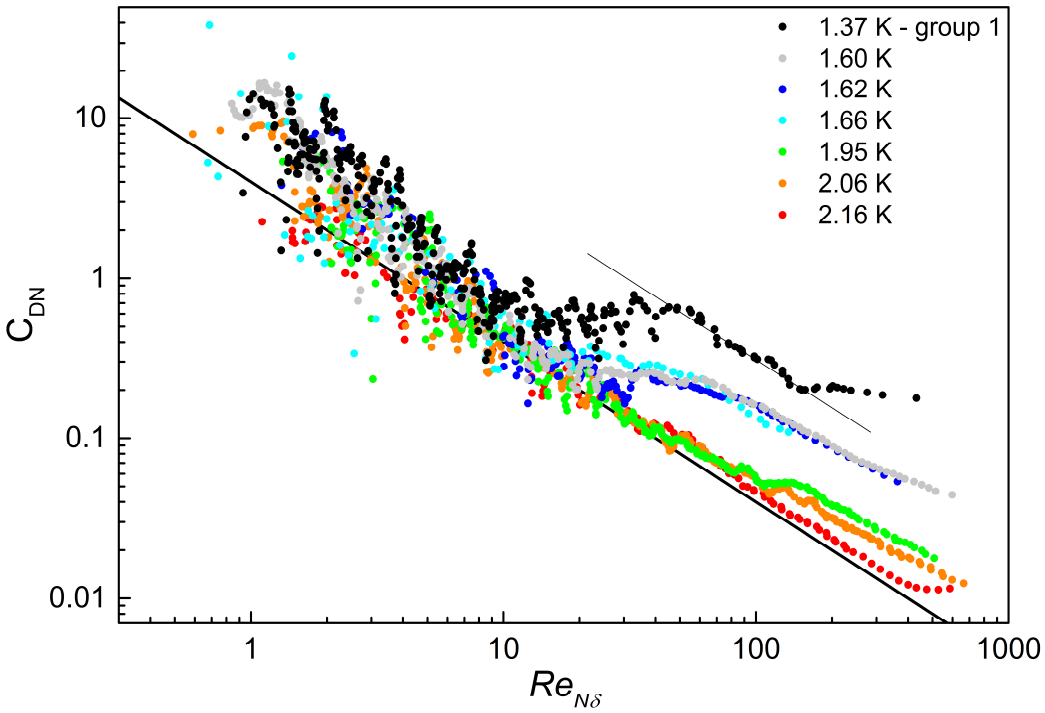

Fig. 3.13: The drag coefficient for the normal component plotted against the Reynolds number defined for the normal component using the viscous penetration depth, δ. This collapses the low amplitude drag forces, proving that this force originates from the laminar component and that we are indeed operating the oscillating disc in the high frequency limit, as mentioned in section 1.3. Without any significant error, we can consider the dependence taken at 2.16 K to correspond to the behaviour of the normal component alone. The parameter $Re_{N\delta}$ is the only relevant dimensionless flow parameter in the high frequency limit. If only the normal component were involved in the flow (laminar or turbulent), all data should have collapsed to a single dependence similar to the data taken at 2.16 K. Thus, any departure from the data taken at 2.16 K is again shown to be necessarily due to the action of the superfluid component. As this plot does not collapse the dependence above the lower critical angular velocity, it is now clearly shown that a second quasi-laminar flow exist again for all temperatures below 2 K. The upper critical velocity is shown reliably only for 1.37 K. The purpose of the solid lines is the same as in figure 3.12.

A synthesis of all the information gleaned from the presented data allows us to formulate the following likely scenario for the flow of He II around the oscillating disc - valid at least at the lower temperatures (1.37 K, 1.6 K, and 1.95 K). At the lowest angular velocities, the superfluid component stays either at rest or exhibits potential flow (not contributing towards the dissipative forces), while laminar flow of the normal component exists. This laminar flow

is approximately described by the presented theory, except for the differences in the drag forces explained above. The first instability that occurs is due to the emergence of a significant number of quantized vortices in the superfluid component (likely generated from remnant vortices attached to the surface of the disc), and leads to a non-linear increase of the measured drag force that scales with the density of the superfluid component. The presence of these quantized vortices then causes an increase of the mutual friction force (since it acts between the vortices and the normal component) which eventually causes the superfluid component to adapt to the flow of the normal component. We therefore believe that He II exhibits a coupled quasi-laminar flow of both components, resulting in a motion that can be (on length scales exceeding the inter-vortex distance) approximately described as that of a classical viscous fluid with its density equal to the total density of He II and an effective viscosity equal to, or higher than that of the normal component alone (higher drag coefficient). An increase in the effective viscosity might be due to the quantized vortices in the superfluid component also dissipating some part of the kinetic energy, regardless of the specific mechanism by which it occurs. At the highest angular velocities, this quasi-classical fluid will likely eventually undergo further instabilities, as any classical fluid would, triggering the transition to turbulence. This scenario can be found to agree with the original interpretation of Donnelly and Hollis Hallett, although from the current experiment, further information has been obtained about the scaling of the non-linear force. A similar idea has also been discussed and investigated in a recent paper by Skrbek and Vinen summarizing the behaviour of oscillatory structures in He II and ^{3}He-B [21].

Having described the scenario which can be advocated convincingly based on the presented data, it is also fair to say that if one considers the non-ideal motion of the disc, the noise levels at low amplitudes and other adverse effects, this scenario should perhaps be thought of as a likely possibility rather than well-proven fact. Nevertheless, a very similar scenario was formulated for the behaviour of quartz tuning forks in He II in the same temperature range [9], where efforts were also made to quantify the degree of coupling between the normal and superfluid component. Although the data presented in ref. [9] are less affected by noise and similar effects,

at the time they have not been processed in the same fashion as in the present work and do not seem to show the two laminar-like flow regimes too convincingly.

3.3 Suggestions for Improving the Experiment

For future work on the oscillating disc, it would be desirable to focus on the following aspects: It would be appropriate to use a heavier, more stable glass disc mounted on the fibre at an angle as close to 90 degrees as possible. It would also be advisable to improve the contrast, reliability and spacing of the marks on the disc. For example, the choice of a dark opaque paint would significantly help to increase the contrast of the dots against the background, which could be complimented by better lighting inside the cryostat as well.

It will be necessary to reduce any mechanical vibrations due to the pump; For example, this could be done by selecting a longer, more flexible hose and by fitting the cryostat with rubber dampers. Unwanted lateral vibrations should be limited even more by an adapted drive mechanism, as the present manual one may cause significant vibration during the initial movement, leading to increased noise. Such a drive mechanism should also allow higher initial amplitudes, which would also be essential in determining when the coupled components become turbulent at higher temperatures.

After these improvements are made, it would also be possible to think of better data processing methods. For example; to allow a more precise determination of the actual angular displacement, rather than angular velocity only, which is its derivative and thus is more prone to random noise.

It would also be interesting to change the disc diameter and compare the behaviour, or perhaps to design a similar experiment with another axially symmetric body such as a sphere or cylinder and to compare with available results or even between different shapes of the torsionally oscillating bodies.

Conclusions

After finishing all necessary tests at room temperature and at liquid nitrogen temperature which led to significant improvements of the apparatus and data acquisition, measurements with a torsionally oscillating disc were performed in superfluid helium at temperatures between 2.16 K and 1.37 K at saturated vapour pressure. We were able to measure the time dependence of the angular velocity of the disc and to determine a critical value of the angular velocity amplitude. The obtained temperature dependences also provide information on what the nature of the observed instabilities is likely to be.

We have presented evidence showing that the measured non-linear forces originate from the superfluid component, which is an improvement over the original interpretation of a set of similar experiments performed by Donnelly and Hollis Hallett [7], where a similar concept called the “entrainment of the superfluid component” was presented, which seemed to be halfway between an assumption and experimental fact. Moreover, the described effect was not at all present in the data shown for the single oscillating disc, as sufficiently high amplitudes have not been reached. Thus, as far as we know, for the case of the single oscillating disc this is a new result and we are not aware of any previous work that would show the same.

Based on our experience with other oscillatory structures, we have proposed a detailed scenario of the transition to turbulence for this experimental arrangement and present evidence in support of its validity within the limits of experimental accuracy, forming an overall picture of the characteristics of the flow of He II around a torsionally oscillating disc. This scenario is generally in agreement with the conjectures drawn by Donnelly and Hollis Hallett, but is now laid down in greater detail and supported by additional experimental results. Nevertheless, there is always room for improvement, and the torsional oscillator experiments will continue to be studied in the Superfluidity Laboratory.

Bibliography

1. **Kapitza, P.** 141, 1938, Nature, p. 74.
2. **Allen, J. F. and Misener, A. D.** 141, 1938, Nature, p. 75.
3. **Burton, E. F.** 135, 1935, Nature, Lond., p. 265.
4. **Andronikashvili, E. L.** 10, Moscow : s.n., 1946, Journal of Physics, p. 201.
5. **Landau, L. D.** 5, 1941, J. Phys. USSR, p. 356.
6. **Landau, L. D.** 11, 1947, J. Phys. USSR, p. 91.
7. **Donnelly, R. J. and Hollis Hallett, A. C.** 3, 1958, ANNALS OF PHYSICS, Vol. 3, pp. 320-345.
8. **Blaauwgeers, R., et al.,** 5-6, 2007, J. Low Temp. Phys., Vol. 146, pp. 537-562.
9. **Blazkova, M., et al.,** 5, 2009, Phys. Rev. B, Vol. 79.
10. **Schmoranzer, D., et al.,** 6, 2010, Phys. Rew. E, Vol. 81.
11. **Landau, L. D. and Lifshitz, E. M.** *Fluid mechanics.* s.l. : Pergamon Books Ltd., 1987. 0-08-033933-6.
12. **Dzyaloshinskii, I. E., Lifshitz, E. M. and Pitaevskii, L. P.** 10, 1961, Adv. Phys., p. 165.
13. **Allen, J. F. and Jones, H.** 141, 1938, Nature, p. 243.
14. Lecture Notes in Physics. [book auth.] W. F. Vinen. [ed.] C. F Barenghi, R. J. Donnelly and W. F. Vinen. *Quantized Vortex Dynamics and Superfluid Turbulence.* s.l. : Springer Berlin Heidelberg, 2001, Vol. 571, pp. 149-161.
15. **Bowley, R. M. and McClintock, P. V. E.** *Progress in Low Temperature Physics.* s.l. : Elsevier, 1995. Vol. 1.
16. **London, F.** 141, 1938, Nature, p. 643.
17. **Tizsa, L.** 141, 1938, Nature, p. 643.
18. **Osborne, D. V.** 368, 1950, PROCEEDINGS OF THE PHYSICAL SOCIETY OF LONDON SECTION A, Vol. 63, pp. 909-912.
19. **Arp, V. D. and McCarty, R. D.** 1998. INTERNATIONAL CRYOGENIC ENGINEERING CONFERENCE 1998. pp. 47-55.
20. **McCarty, R. D.** *Thermophysical Properties of Helium-4 from 2 to 1500 K with Pressures to 1000 Atmospheres.* s.l. : National Bureau of Standards, 1972. Technical. Technical Note 631.
21. **Vinen, V. F. and Skrbek, L.** 25 Mar 2014, Proc Natl Acad Sci U S A, Vol. 111(Suppl 1), pp. 4699–4706.